Cryogenic Vacuum In-Situ Device Calibration:

A Trade Study

by

Marko Neric

A Thesis Presented in Partial Fulfillment
of the Requirements for the Degree
Master of Science

Approved April 2023 by the
Graduate Supervisory Committee:

Georgios Trichopoulos, Chair
Chris Groppi
James Aberle

ARIZONA STATE UNIVERSITY

May 2023

ABSTRACT

I present a trade-study of methods for a 1-port vacuum cryogenic in-situ calibration of a vector network analyzer. The three main methods I investigated in this work were: calibration using a commercial off the shelf latching electro-mechanical six way switch, a custom switch board, and a flexible multi channel stripline based printed circuit board. The test procedure was developed for use in a ground based closed-cycle cryogenic test bench to measure the reflection coefficient of a single port connectorized device under test. The device was installed in the cryogenic system alongside calibration standards. The goal of the trade study was to find which method could be used to accomplish calibration and device measurement in a single thermal cycle. Four cycles were required for industry standard open-short-load device calibration. Room temperature measurements were done with all three calibration schemes but ultimately only the single pole six throw switch proved effective enough for further testing. The cryogenic testing was carried out on an arbitrary device at $\sim$ 3K temperature, over a 6 GHz bandwidth. The final objective was to develop a setup and procedure for measuring the frequency and temperature dependent complex impedance of superconducting devices such as hot electron bolometer mixers, which are used for down converting the signal in the IF chain of astronomy instruments. Characterization of superconducting devices while they are at their operating temperature is challenging using traditional calibration methods. This commercial alternative is less expensive and more efficient in terms of thermal cycles and set up because it can be installed in a wide variety of cyrogenic systems.

TABLE OF CONTENTS

LIST OF TABLES

Table Page

LIST OF FIGURES

Chapter 1

INTRODUCTION

1.1 Science Background and Motivation

This work was largely motivated by the engineering challenges faced in mm and sub-mm astronomy instrumentation. This field of astronomy is concerned the observations of electromagnetic (EM) radiation that falls into the frequency range of 0.10 to 10.0 terahertz (THz). This range is particularly useful for studying the interstellar medium (ISM) which is all the material found between stars that cools by emitting light. That material is largely hydrogen (H), and helium (He) which combined make up $\sim$ 98 % of the gas in the ISM with carbon (C), nitrogen (N), oxygen (O), and heavier metals contributing to the remainder. H observations can serve as a diagnostic for neutral atomic or ionized gas, while He is mostly non-interacting. What makes the latter three atomic species so important is that their cooling comes in the form of forbidden fine structure emission that can even permeate dense regions and outshine H. These lines are denoted with roman numerals to indicate the state of the atom where numeral I is for a neutral state, and II for the first ionized sate. So, singly ionized carbon can be written [CII] and it will emit light of wavelength 158 μm, or frequency 1.89 THz. [CII] is very bright in the ISM and due to the fact that C requires less energy to excite and ionize than H, it can even shine where H is totally neutral. Ionized carbon measurements combined with observations of [NII] 205 μm (1.46 THz), and [OI] 63 μm (4.75 THz) can provide details about physical distribution of ISM components, and the chemistry, and physics actively going on there. Despite this, the field of sub-mm

astronomy is lagging behind other astronomical divisions. This is because the THz frequency range is also known as the THz gap. This is a gap in technology where sources to produce and carry high frequency signals in the laboratory environment have only recently become available. The Earth's atmosphere does not cooperate with THz astronomers, as most frequencies of interest are absorbed before they reach the ground.

Even with lab sources, and space/high altitude observing platforms, sub-mm signals from line emission are too high frequency for most modern electronics. A technique called heterodyne mixing is used to produce lower frequencies. In heterodyne mixing two signals of different power are convolved, or mixed, together in a non-linear device. The non-linearity means that it has an IV curve which deviates from the linear form of Ohm's law: V = IZ. For THz astronomy the two signals are an incident sky signal and a local oscillator (LO) lab source. Taking advantage of the nonlinear properties of superconducting materials allows us to down convert THz emission into an intermediate frequency (IF) band. Some of these non-linear devices are superconducting sensors like the superconductor-insulator-superconductor (SIS) mixers (Zmuidzinas and Richards 2004), and for frequencies greater than 1 THz there are hot electron bolometers (HEB) (Gousev et al. 1994). The HEBs are typically made from niobium nitride (NbN) (Khosropanah et al. 2007), or recently from magnesium diboride (MgB_2) (Cunnane et al. 2014). The mixers are usually a thin film of the superconductor of choice, bridging the leads of a spiral antenna. In the case of some HEB mixers, the spiral antenna is wire bonded to a transmission line (TL) that terminates in an output port where a bias-tee carries signal and drives the mixer.

These devices must be brought below a critical temperature (T_C) in order for the material to be superconducting. Thus mixers are installed in vacuum cryogenic

systems. When incident THz signals arrive at a receiver, they arrive with low power. After heterodyne down-conversion the signal must be amplified to be detected. The amplification process usually comes from cryogenic wide-band low noise amplifiers (LNAs) (Weinreb, Bardin, and Mani 2007). There will always be some inherent impedance mismatch between the mixer output and LNA input. The mismatch can cause standing waves in the IF system. These standing waves can be so severe they cause the loss of the already weak signals or complicate the data reduction process which produces the final astronomy images. This becomes an interesting electrical engineering problem because the natural solution is to measure the impedance of the two components and build a matching network between them that maximizes the power output. However, the device characterization is non-trivial when the device-under-test (DUT) is physically sealed in a vacuum chamber, and brought to low Kelvin temperatures. The industry standard calibration system requires the use of a vector network analyzer (VNA). The calibration of the VNA removes all loss effects between measuring apparatus and the DUT so that the resulting data is of the test device alone. The calibration is done by using reference standards that have already been well characterized, and measuring them with the VNA under the same conditions that the DUTs will undergo. This process is easy to carry out at room temperature where the DUT reference point is in reach, but extremely challenging to do in-situ or in place of a cryogenic chamber.

In this work I present a trade study of three potential methods for accomplishing a 1-port VNA calibration in-situ at sub-10 K temperatures. In the remainder of this chapter I will go over the basics of device measurement and the tools used in analysis. The previous attempts of the community to characterize HEB mixers is discussed in section 1.2. Standard things like the scattering matrix is discussed in

section 1.3, basics on how measurements are obtained and displayed are in section 1.4, and basics of VNA calibration can be found in section 1.5. The following chapter details the initial room temperature external calibration tests of various schemes. The first two attempts at measurement were novel setups. One using a custom single pole quad-through (SP4T) switch board that will be discussed in section 2.2, and a flexible printed circuit board (PCB) ribbon detailed in section 2.3. The best (and only) performing cryo calibration setup involves using a commercial off the shelf (COTS) RF switch which I show initially in section 2.4. The cryogenic testing is discussed in section 3.1, and the future work related to these projects is discussed in chapter 4

1.2 Previous Work

Previous attempts of in-situ VNA calibration have been made to varying degrees of success. The key challenge being that the DUT is physically isolated from the VNA and operator. Electronic calibration kits are a staple of the RF engineers tool-set but are non-functional at cryogenic temperatures. Independent manual standards can be applied by hand at each VNA port when the measurement site is accessible but this is not possible inside the cryostat. Alternatively, the individual standards could be installed in place of the DUT and measured one at a time as the cryostat is cooled-down and warmed-up henceforth known as a cryogenic cycle. This process is not totally outrageous, but for a one-port calibration this will require a minimum of three standards. This will ultimately take three cycles to calibrate and one to measure. The process more than doubles for two-port as that requires an eight or twelve point correction up from three. Even with the fastest systems, manual calibration takes days for a single device measurement. To add to the uncertainty, there is a

change in environment every time the cryostat is opened and components are shifted. Temperature stability is also an issue as different sized objects will change the thermal load of the cryostat and the final measurement temperature could fluctuate. From experience I can state that internal cabling of the cryostat will not rest in the same position between calibration and final measure. Calibrating the VNA by measuring the individual calibration standards over multiple cycles is referred to as the manual method. I used this manual method for validation of my cryogenic results and will discuss it further in section 3.1.

Contact probe stations can measure impedance across multiple points on an object. The probes can be externally controlled so they have a potential for use in cryostats for devices without a connector, like thin films and chips. They are costly however, and suffer mechanical failure at extremely low temperature. Radio frequency (RF) switches are another potential solution for in-situ calibration but they usually require heavy modification to be used at low temperature. Only recently has a commercially available cryogenic rated switch become available. Though modern RF switches are designed so that electrical lengths between channels are roughly equivalent, there will always be some deviation. Since a calibration is normally done using the same cable between VNA and device, there will be uncertainty in the correction using a switch since not all paths will look the same to the RF signal. This can be corrected for by measuring the trace differences, but for lower frequency measurements the difference can be negligible. Switches also require DC biasing to actuate. This can be a challenge in some closed systems. Any wiring adds to the thermal load, so it is not common to have an excess of available DC wires beyond what is needed to power the DUT.

Several microwave and superconducting devices have been measured using custom through-reflect-line (TRL) boards and switches for two-port devices (Diego 2010;

Slichter 2011; Ranzani et al. 2012; Ranzani et al. 2013) but these are not industry standard calibration references, and these techniques were more focused on impedance measure of individual components that will match to a larger circuit. Some required additional software corrections. The mixing element of an IF system will be connectorized. Meaning the enclosure housing, and output port will contribute to the overall impedance not just the thin film or antenna and must be measured together.

Rodriguez-Morales and Yngvesson (2003) took noise and impedance measurements of an HEB at 4 K, however their device was not bonded to an antenna and therefor not the total device impedance. Kooi et al. (2007) measured an HEB using the mixer itself as cal standards. The device was treated as a known load when above 20 K, and a short below T_C. This was an interesting approach because it exploited the fact that a superconductor will have 0 DC resistance below critical temperature. Again, this approach does not use industry standards or the minimum of three references for a one-port calibration. To date the most accurate measurements were done by Rodriguez-Morales, Yngvesson, and Gu (2010) where the authors did a manual open-short-load (OSL) cal over three cycles to measure an HEB mixer and compare to theoretical models. My proposed calibration setup was a way of diminishing the time consuming nature of that test, and added uncertainty of the manual cal. In this work I recreate their manual calibration at cryogenic temperatures, and introduce a single cycle method applied to a generalized DUT which can be easily replaced with a superconducting device for a wider band calibration (section 3.1). The following sections are basics about device characterization.

1.3 S-Parameters

Objects that can send and receive electrical signals are modeled as N-port networks where N is the number of inputs and outputs of the device. Some examples are passive, like wires, and cables that transmit various signal frequencies as a two-port device. Describing these networks as a series of matrix interactions makes them easier to understand qualitatively and quantitatively. Ohm's law for a multi port network can be written as impedance matrices $\mathbf{V} = \mathbf{ZI}$ where $\mathbf{Z}$ is a matrix and has elements Z_{mn} based on the matrix indices. The is well covered in the microwave analysis chapter 4 of Pozar 2011. This is not the only possible matrix representation of a microwave network. One can use block diagrams when analysing EM interactions with multi-port networks like the one represented in Figure 1(a). This model represents a two port device with incident and reflected traveling waves at port one: a_1, and b_1 respectively. Also for port two there is an incident a_2 wave, and reflected wave b_2. The traveling waves are defined in Kurokawa (1965) for a general incident wave at port i. These traveling waves can be related to power by the square of their magnitude, i.e. incident power is $P_i = |a_i|^2$ and reflected power $P_r = |b_i|^2$. Figure 1b is a signal flow diagram of the same system. Here are shown a set of parameters that describe incident and reflected waves relative to each another. In terms of the two-port network the interactions with the independent ports are denoted S_{ii}, and S_{jj} while the forward and reverse interactions are S_{ji} and S_{ij}. This diagram can be expressed as a 2×2 matrix like that of equation 1.1:

$$\begin{pmatrix} b_1 \\ b_2 \end{pmatrix} = \begin{pmatrix} S_{11} & S_{12} \\ S_{21} & S_{22} \end{pmatrix} \begin{pmatrix} a_1 \\ a_2 \end{pmatrix} \tag{1.1}$$

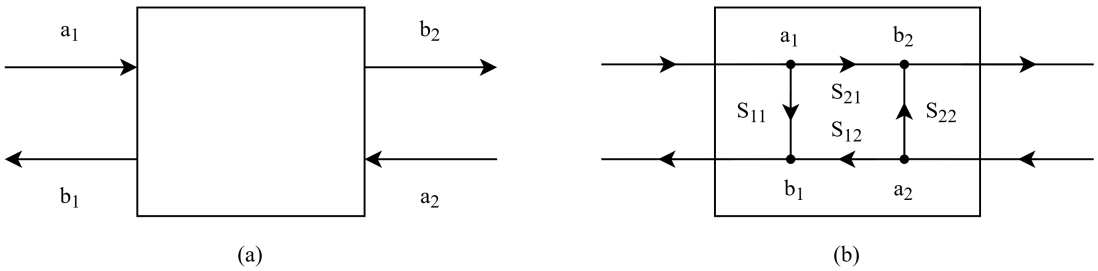

Figure 1. Power Waves Diagram

Note: Figure 1a represents a block diagram of a two port network with incident power waves a_n, and reflected b_n. Figure 1b is the same diagram but in signal flow terms. This image relates the power waves to the scatter S matrix.

Using matrix multiplication, the port 1 traveling wave can then be written as:

$$b_1 = S_{11}a_1 + S_{12}a_2 \tag{1.2}$$

Measurements of the scattering matrix parameters are done under the following conditions. First the output port is terminated with a load impedance equal to the intrinsic impedance. Next, a source signal is sent to input port one. A terminated port with a matched load Z_0, will not transmit signal so with nothing driving it the input wave of port two vanishes, i.e. $a_2 = 0$. Then one could solve for the first S-parameter S_{11} (read out loud as: "S-one-one"):

$$S_{11} = \left.\frac{b_1}{a_1}\right|_{a_2=0} \tag{1.3}$$

The same process can be done for the other S-parameters. Under the constraints of S-parameter measurements the traveling waves can instead be written as simply traveling voltages. For the case of the incident the general expression is: $a_n = V^+$. For reflected one can write $b_n = V^-$. The standard convention for direction is that the negative sign (-) implies signal reflected from a port, and the (+) is for signal incident on a port which carries over directly from the original definitions of b, and a. The scattering matrix is a mainstay of RF engineering. From Pozar (2011) it can be used in general form as:

$$\mathbf{V}^- = \mathbf{S}\mathbf{V}^+ \tag{1.4}$$

$$S_{ij} = \left.\frac{V_i^-}{V_j^+}\right|_{V_k^+ = 0 \text{ for } k \neq j} \tag{1.5}$$

Where equation 1.4 uses bold text to identify the variables as matrices. Looking back at equation 1.3 now means that S_{11} is found by driving port 1 with an incident

wave of voltage V_1^+ and measuring the reflected wave amplitude V_1^- coming out of port 1. While that measurement is happening all other ports are off i.e. terminated with matched loads. The gain for a two port device would be calculated from S_{21}. It is important to know that S_{11} is the reflection coefficient, which is interchangeable with the variable Γ. This relates the intrinsic impedance Z_0 to the load impedance Z_L

$$S_{11} = \frac{Z_L - Z_0}{Z_L - Z_0} \tag{1.6}$$

The variable Z_0 as mentioned before is an intrinsic system impedance which is typically designed to be 50 Ω for microwave engineering. S_{11} and Z_{in} are complex numbers. S-parameters are generally calculated in units of decibels (dB) which converts them from a linear to a logarithmic scale as shown in the following equation:

$$\text{dB} = 10\log_{10}\left(\frac{P_i}{P_j}\right) \tag{1.7}$$

This expression is used for power ratios where P_i and P_j are in units of W. A dB then is a relative unit where either input or output power may not be known. If instead a results is given in dBm, then the power received by the load is set to P_j = 1.0 mW. Power ratios can be thought of in terms of voltage ratios from the fact that power: P = IV. I is current, and V is electric potential or voltage. From Ohm's law V = IZ where Z is complex impedance. Then one can express power in terms of voltage $P = V^2Z^{-1}$. Combining equations 1.5, 1.7, and using exponent rules for logarithms, with a matched impedance, allows for dB to be defined as the ratios of voltage:

$$\text{dB} = 20\log_{10}\left(\frac{V_i}{V_j}\right) = 20\log_{10}\left(S_{ij}\right) \tag{1.8}$$

Expressing the S-parameters as decibels allows problems that would normally require multiplication and division to be done with simple addition and subtraction

A few additional, and very important terms in microwave engineering are the insertion loss (IL), and return loss (RL). Insertion loss describes how much signal transmitted was not received. This is the loss effects that occur from "inserting" or connecting to a component. IL is related to gain by:

$$\mathrm{IL(dB)} = -20\log_{10}\left|S_{21}\right| \tag{1.9}$$

The word loss already implies that there is a decrease in transmission so the negative sign in the above equation prevents redundancy from one saying "-20 dB of loss." Likewise, return loss measures the loss of an incident traveling wave to the reflective of the same port. It is related to S_{11}:

$$\mathrm{RL(dB)} = -20\log_{10}|S_{11}| \tag{1.10}$$

Another concept is Isolation. This is a measure of how well the ports of a system are shielded from one another. Sometimes called the cross-talk, or isolation, in an ideal system would mean that when a single channel of a multi-port device was active, no signal would be measured in adjacent or nearest neighbor channel. An example being that $S_{21} \neq 0$ for an N + 2 system would mean that $S_{31} \ll 0$.

1.4 VNA Measurement

The VNA is the workhorse of RF electronics. This is a resource commonly used in device characterization. The VNA works as an RF source that can sweep over different frequencies and output power that can characterize a device by measuring the S-parameters. A VNA is usually comprised of a source with a switch controlled forward or reverse orientation, and directional couplers to isolate incident and reflected

waves. A local oscillator converts the RF signal to an intermediate frequency IF for the desired measurement band. A schematic for a two-port VNA has been reproduced from Rytting (2001) and can be seen in Figure 2. The RF source is switched in the forward direction such that the traveling wave a_1 is incident on port 1 of a two-port DUT. The second port of the DUT is terminated by a matched load that is engaged when the RF source switches from reverse to forward direction. Couplers isolate the lines and transfer the net waves of a_1, b_1, and b_2 to mixers that are pumped with LOs. The waves read by the VNA electronics are a_0, b_0, and b_3 that are down converted linearly scaled version of the previously mentioned traveling waves. S_{11}, and S_{21} measurements are possible with this configuration, and when the switch reverses its flow the remaining two-port S-parameters are measured. I have already discussed how S_{11} relates to system impedance but, for a 1-port measurement it can be written more precisely as in Rodriguez-Morales (2007):

$$Z_{\mathrm{L}} = Z_0 \frac{1 + S_{11}}{1 - S_{11}} \tag{1.11}$$

Z_L and S_{11} by extension are complex, i.e. $Z = R + jX$ where R is the real resistive component and X is the imaginary reactance that comes from inductance and or capacitance, and $j = \sqrt{-1}$ is the imaginary number. Complex numbers are usually expressed on an xy plot where the x axis is real, and y is imaginary. Most modern VNAs have software installed for recording and displaying measurements. They can be output in rectangular charts where the S-parameters are drawn with respect to frequency for example, but another tool exists for visualising the complex impedance known as the Smith Chart. This chart is an extension of the two dimensional real and imaginary plots but here the imaginary axis is warped into a loop. Figure 3 is one of the most useful images ever made. The smith chart works with a normalized

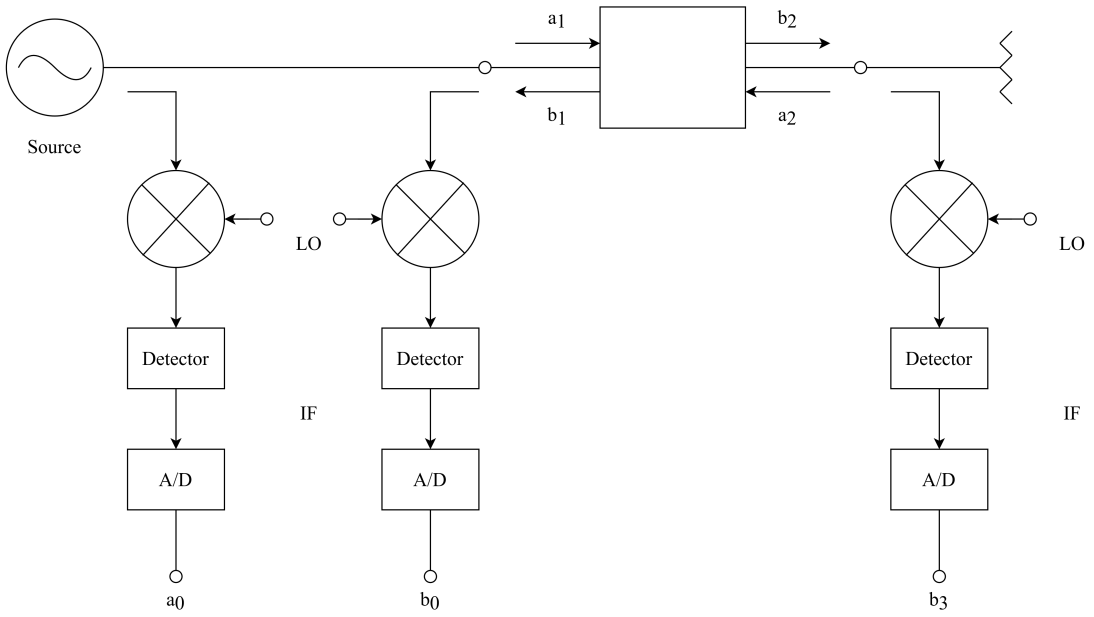

Figure 2. Two Port VNA Schematic

Source: Rytting (2001)

Note: A diagram of a forward direction (signal from port 1 to port 2) coupled VNA. This image shows the paths of incident traveling waves a_n, and reflected b_n through a two-port device. The switch provides a matched load termination for port 2. The IF produced by RF and LO mixing is transmitted through to a detector and an analog-to-digital converter reads out the signals as a_0, b_0, and b_3 for the source reflection, device reflection, and device transmission respectively

impedance which is $z = Z_L/Z_0$. Specific points of interest are highlighted in the figure like where an open, short, and matched load would come to rest on the chart. The major benefit here is that the smith chart is a graphing tool that when used correctly will give the necessary impedance a matching network would need to adjust for.

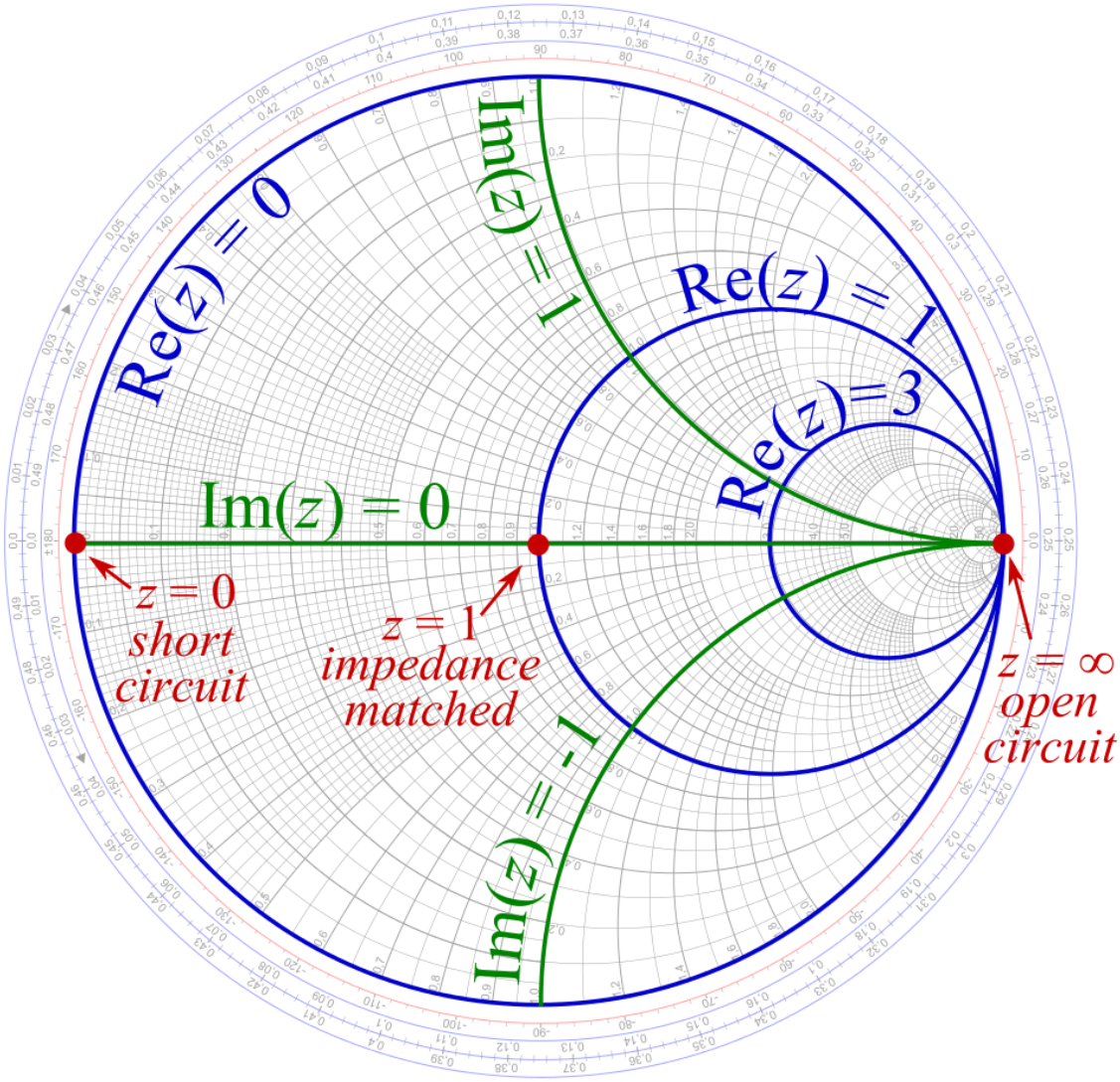

Figure 3. Smith Chart

Source: https://www.digikey.com/en/articles/the-smith-chart-an-ancient-graphical-tool-still-vital-in-rf-design

Note: Pictured here is a smith chart used to plot normalized complex impedance. The tool is often used when building matching networks between interconnects. The smith chart is an elongated form of the real and imaginary axes for complex numbers. The x-axis is totally real, but the y-axis has been stretched along a circle. The highlighted lines mark where important cross-overs happen. A purely resistive 50Ω load would rest on the dot marked z = 1. Any reactance would drive the dot above or below the real plane but along the curve marked Re(z) = 1.

1.5 VNA Calibration

There are several factors in the accuracy of VNA measurements. Not the least of which is the calibration. VNAs will have a standard factory calibration that brings the measurement reference plane to the output of the VNA ports. This means that everything after the port is what the VNA measures. In the most straightforward setup a coaxial cable will extend from a measurement port to the DUT. The S matrix recorded by the VNA will include the losses due to the cable length, and any impedance mismatch between the VNA-cable-DUT system. That mismatch can be modeled using the same principles as in Figure 1(b) where the additional effects of the cable are treated as a separate error network seen in Figure 4. The goal of VNA calibration is to characterize the error network. This is accomplished by measuring devices for which the response is well known to the VNA. There are many different calibration setups but the ones I will discuss are the TRL method mentioned in section 1.2, and OSL which is the primary cal setup I will use. TRL standards are a short transmission line known as a through, a terminator known as a reflect, and a documented length of transmission line to be longer than the through. The advantage is that this can calibrate two ports with three standards, but it can be limited in bandwidth. The OSL method requires an open circuit, short circuit, and matched load. This method is meant for one-port calibrating but can be extended to a two port calibration if each port is shown the OSL and then a fourth cal standard, the through, is added between cables. OSL kits can be found for various connector types. This is useful for measuring one-port impedance of a fully packaged and connectorized device.

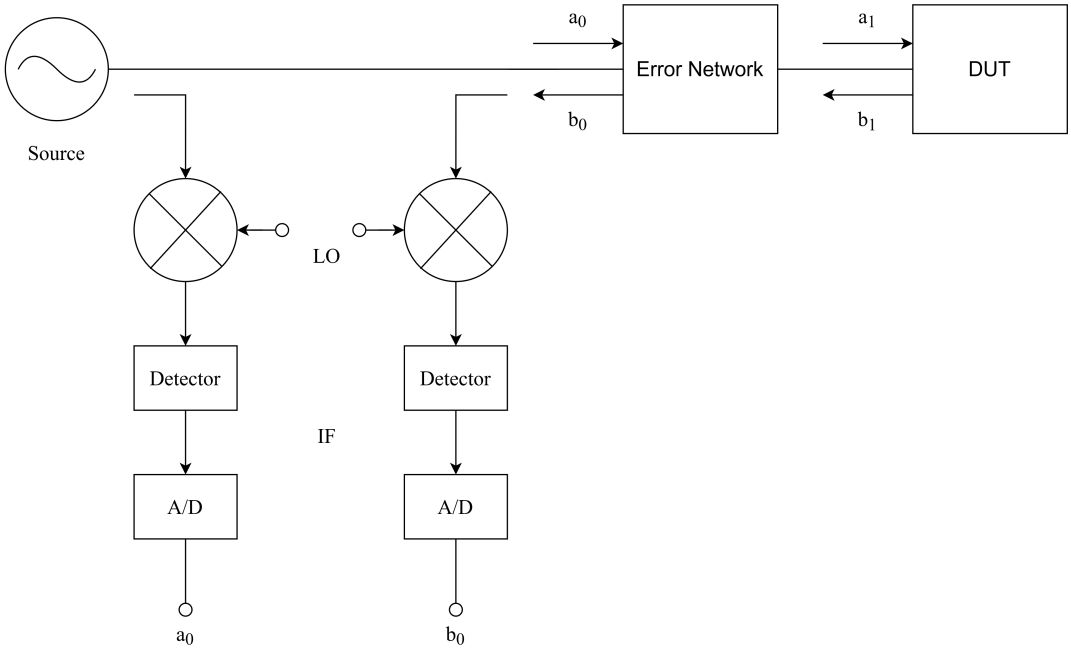

Figure 4. One Port VNA Error Diagram

Source: Rytting (2001)

Note: A 1-port VNA block diagram with an error network that arises from raw measurements.

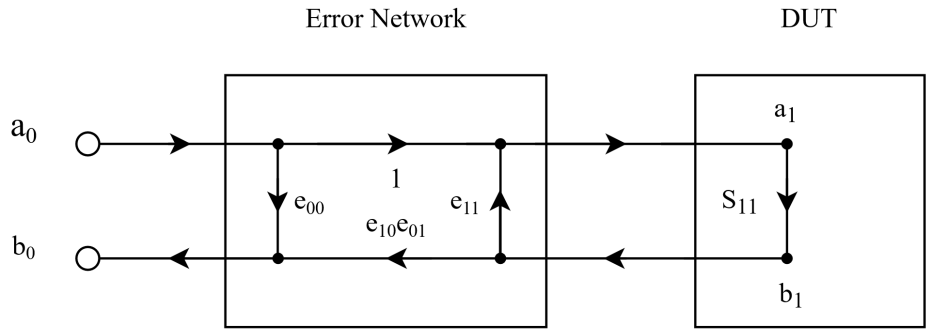

Figure 5. One Port Error Matrix

Source: Rytting (2001)

Note: The signal flow diagram of figure 4. This shows the error matrix terms that can be corrected for to measure the DUT.

Figure 4 can be modeled with a signal flow diagram, as shown in Figure 5. The parameters that run through the error network are the ones that need to be adjusted for to move the reference plane of the VNA to the DUT. The error matrix for a one-port device will require a three-term correction. This is significantly easier than the 12-term correction of a two-port network. The three terms are: e_{00} known as the forward directivity, e_{11} is the port 1 match, and $e_{10}e_{01}$ is known as the forward reflection tracking (Diego 2010). Each of the terms ultimately measure loss interactions through the error network and VNA like the forward directivity which is a ratio of measured loss between source and b_0 and loss between source and a_0. The full error correction is done by matrix operations and detailed in Rytting (2001) which I have reproduced in the following equations (recall $S_{11} = \Gamma$).

$$e_{00} + \Gamma\Gamma_{\mathrm{M}}e_{11} - \Gamma\Delta_{\mathrm{e}} = \Gamma_{\mathrm{M}} \tag{1.12}$$

Where Γ is the actual reflection coefficient of the the DUT, and $\Gamma_{\mathrm{M}} = \frac{b_0}{a_0}$ is the measured value from the VNA. Δe is a simplified error term:

$$\Delta_e = e_{00}e_{11} - e_{10}e_{01} \tag{1.13}$$

Equations 1.12, and 1.13 demonstrate why three standards are the minimum for effective accuracy. There are three unknowns: e_{00}, e_{11}, and Δ_e. Γ_{M} is obtained by raw measurement of the VNA through the error matrix. If three independent objects of known Γ are measured with the same error matrix, then the three terms can be solved for. The error matrix can then be subtracted. Ambient temperature, cable positioning, and other environmental conditions can influence the accuracy of calibration. The DUT can contract and change conductivity as temperatures lower. The error matrix will not be the same then as it was for the room temperature calibration. This results in a calibration drift which is why in-situ calibration is desirable for cryogenic measurements.

Chapter 2

INITIAL ROOM TEMPERATURE MEASUREMENTS

2.1 Test Device and Standards

Whatever schemes are devised for in-situ cryogenic calibration they will have to be validated at room temperature first. There is no reason to believe a method that does not work under normal operating conditions will suddenly get the job done at cryo. For the first set of measurements I made an RLC circuit that would serve as a DUT. I chose surface mounted SMD lumped element components that were known to work at single digit Kelvin temperatures. I simulated an ideal RLC response in Keysight Advanced System Design software first, and then added touchstone files with S-parameter measurements of individual components from the manufacturer's library. The final circuit would vary from simulation, however I wanted to make sure the resonant frequency f_0 of the device would be below 6.00 GHz. The assembly device was wrought with peril. The transmission line was a grounded co-planar waveguide (GCPW) made from Rogers material. The intent was that these boards would be a through board. Any circuits built on them would need to have the center conducting trace of the CPW cut and peeled away with a knife so componentes would not short. This, believe it or not, was a cheaper alternative to buying RF kits that came with various lengths of transmission line meant to be glued together to make RF paths in a circuit. The CPW boards were meant to fit in a small copper package used for cryogenic LNAs designed by Mani and Mauskopf (2014). The package I used was not that, so the transmission board had to be stacked in height so that the top layer could

reach the SMA output. A side panel SMA termination was secured to the box, and then soldered to the CPW. The final components were an 0603 Susumo resistor $\sim$ 50 Ω, a series 0402 Murata capacitor $\sim$ 100 pF, and a shunt inductor $\sim$ 3.9 nH from CoilCraft. The stacking of boards resulted in excess solder flowing through a series of ground vias. The second port of the device package was not connected, although a small segment of the line continues past the inductor which creates an open stub. The assembled Frankenstein's circuit is pictured in Figure 6.

I did all measurements using a Rhode & Schwarz ZVA 24 Vector Network Analyzer that had been certified factory calibrated in the last four years. I used multiple calibration standards for room temperature validation. The most accurate and efficient kit was an electronic ZV-Z52 electronic calibration kit (ECAL). The ECAL was a four port device that could calibrate all of the VNAs ports at the same time. This was too valuable, and far too bulky to put in a cryogenic system. I also used individual manual calibration kits from Keysight. A certified 85033E DC - 9 GHz SMA kit was available. This was also too valuable to use at cryogenic temperatures, especially when the approximately $5000 kit was only rated to -15 C and the DUT would be at $\sim$ -270 C. A used 85033D cal kit rated from DC - 6 GHz with 3.5 mm SMA adaptors was purchased off of eBay. The key difference between the two manual sets is the frequency range. For calibration purposes all other factors were equivalent. To validate the test standards I measured several RF devices at room temperature using both the E/D kits and compared. Over the 6 GHz bandwidth there was no appreciable difference.

The actual calibration standards in the kit come sealed in a cylindrical carousel. Each one can be removed from the holder. This was necessary since the standards would need to be thermally coupled to a cryogenic test bed. The holder was not very

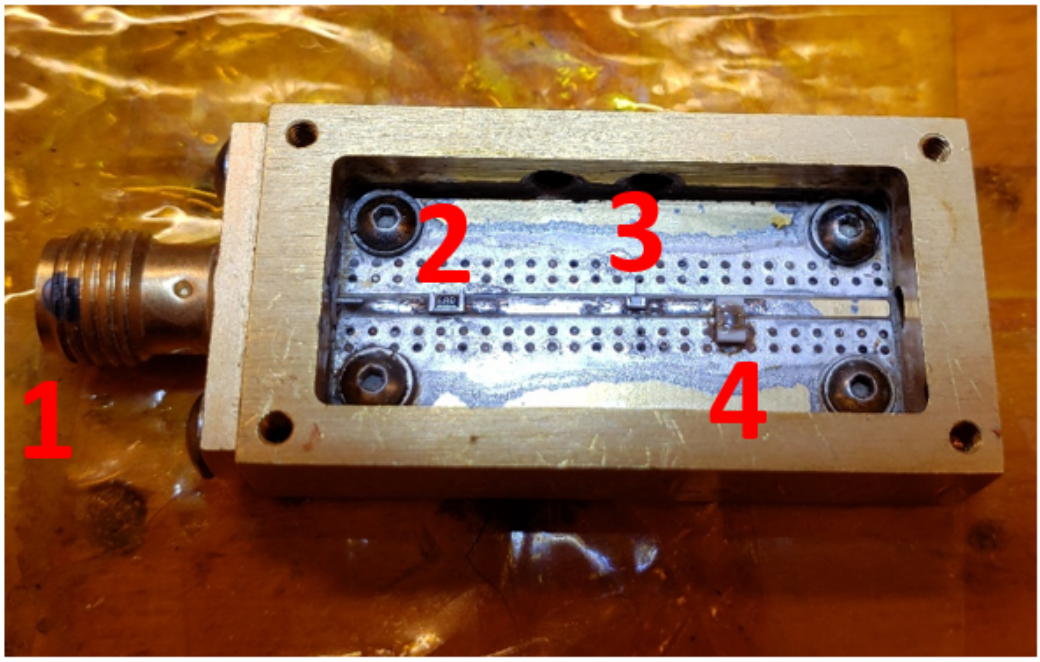

Figure 6. RLC DUT

Note: The generic DUT used in initial testing was an RLC circuit. The single port was a panel mounted SMA (1). The circuit was assembled with a resistor (2) R = 50 Ω, and inductor (3) L = 3.9 nH, and capacitor (4) C = 100 pF. The board used was a grounded co-planar waveguide (GCPW) line matched to 50 Ω. The device package was re-purposed from a cryogenic LNA. The boards need to be extended to reach the SMA outputs which lead to an excess of solder.

thermally conductive, and it had the combined mass of all three standards with empty space inside. The individual standards could be heat-sunk more efficiently when separated. The open, short, and load were detached. All of the room temperature measurements were compared to the ECAL.

2.2 Custom Switch Board (SP4T)

The first approach I tried was to use COTS RF switches. I was previously tasked to investigate how one could expand the access of a cryogenics test bed using switches to increase the number of testable devices. I tested a barrel SP4T for use in a cryogenics setup that might work for multiple devices. That switch did not function at sub 20 K temperatures. Conversely a surface mount switch was a better form factor for thermal load considerations, and might remain operational due to few moving parts. The only ones available were single pole double throw (SPDT). To do cal and measure in a single cycle required a minimum of four channels. I drew a schematic where three independent SPDTs could act as an SP4T. Using the free software KiCad I designed a custom Rogers printed circuit board (PCB) for that purpose. The board had three lands that matched the foot print of the individual switches. The transmission lines were CPW with physical dimensions of width = 25 mils, thickness = 1.4 mils, substrate height 20 mils, and signal trace to ground layer gap of 6 mils to achieve a 50 Ω match. The switches used were Radiall R596832100. These were latching DC - 8 GHz. They required a DC bias of 12 V to actuate. Another version of the same switch was a fail-safe mechanism instead of latching. This was abandoned because it required continuous DC power to energize a path which meant constant thermal input. The latching variant could be pulsed with a short time signal and retain channel orientation. Plated through hole ground vias were used to make an EM fence around the CPW line to isolate the ports from one another. Figure 7 shows one of the completed prototype boards. Side panel SMA connectors were used for RF connections. Small DC pin jacks were used to operate the switch with floating bias. Each switch had its own common input, and two RF paths. The common of the

central switch would act as the incident port of the entire switch board. Selecting the path of the central switch (either left or right) would output RF signal from the central switch to an adjacent switch's common input. The adjacent switch would then transmit the signal out of one of their outputs. The common line C is labeled in Figure 7, along with channels 1-4.

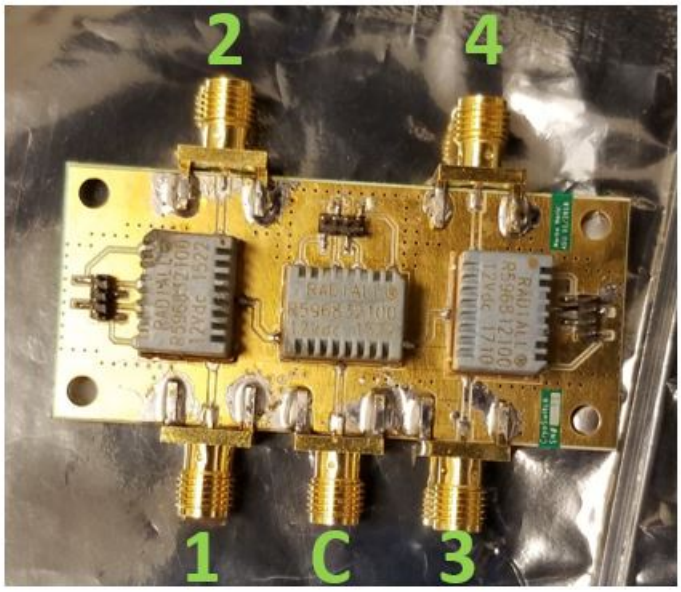

Figure 7. SP4T Switch Board

Note: A custom SP4T I designed to expand channel access in a cryogenic vacuum chamber. The switch uses three Radiall R596 surface mounted SPDT switches. The board in this picture was one of the earlier prototypes. Two of the switches are latching, and the third one is a failsafe. The center switch acts as a common input for the entire network. The two flanking switches change the paths between channels 1-4.

The repeatability of IL between channels of the independent switches were measured. There were notable deviations ($\leq$ 0.15 dB). It was still considered an overall good throughput for S_{21}. The CPW paths between switches were symmetric, however there were some sharp turns that were not well matched for the full bandwidth. The circuit was hand assembled, and the SMA connectors were especially challenging to stabilize during solder. There were some clear signs of non uniformity. This did not present a significant problem in the forward direction, however the reflections suffered for it. Figure 8 shows the transmission (a) and reflections of the SP4T (b). For the prototype there was no shielding beyond the ground vias. The CPW architecture was susceptible to radio frequency interference (RFI). The final version of the switch board was intended to have a full enclosure however, that was not used in testing. The isolation may have been impacted for these reasons. The return loss varied per channel and there was concern variations may result in a bad calibration. Despite some of these drawbacks I attempted a room temperature calibration through the switchboard.

The 300 K test setup was done outside of the cryogenic system. VNA test port power was set to -40 dBm, IF bandwidth of 100 Hz, and measurment frequencies from 0.10 - 6.00 GHz. An individual channel of the board was chosen. I used the 85033D/E open, short, and load standards and and a single mini circuits UT-085 coax cable. The single cable was used so that any uncertainty in path length could be attributed to the performance of the SP4T alone and not additional varying lengths of the coax. I loaded the standards one by one on a single channel: Ch 2. This was done to verify that the individual channels could be de-embedded from the DUT measurement. I then measured the RLC DUT at channel 2 and compared to the independent measurement of the DUT with a cryocal. If there was an appreciable

discrepancy between S-parameters that would mean there was something wrong with the setup or the switchboard could not be de-embedded from the DUT measurement. S_{11} was plotted on a rectangular chart for both measurements and narrow deviation, of ≤ 1 dB, at the resonance was observed. This constituted a maximum of $\sim 1\ \Omega$ difference in the real part of the impedance for $(2.76 \leq f \leq 2.95)$ GHz frequency range between measurements. This was encouraging. If the traces were indeed repeatable then the same calibration on channel 2 would yield a good calibration for channel 1. The first two channels were the opposite path of the same independent switch for this setup. They should be in the best agreement with one another since the internal path of the individual surface mount switch was not changed by the user, and the only difference in assembly at that point is the SMA outputs at the edge of the board. Channel 1 was shown the Ch 2 cal. Here the deviation was much larger not just in depth but over a greater span of frequencies. I repeated the same inspection again using the Ch 2 calibration and measure the DUT at channels 3, and 4. Again the single channel calibration failed to hold.

The most likely cause of these issues are first board design, and second assembly. Figure 9 shows the performance of channels 1 and 2 compared to actual DUT response on the top plot (a), and in the same figure plot (b) shows the results using channels 3, and 4. All measurements deviate starting at 2 GHz. The discrepancy at Ch 1 and Ch 2 indicates assembly issues between output ports. For the case of channels 3/4 there is potentially a design issue in the switch board RF path. The setup would need to be tuned either for length of travel or impedance mismatch between switch ports.

A full calibration was done placing an open standard on channel 1, short on channel 2, matched load on channel 3 and DUT on channel 4. This was more of a mechanical test than anything else as the calibration would obviously fail. The SP4T was loaded

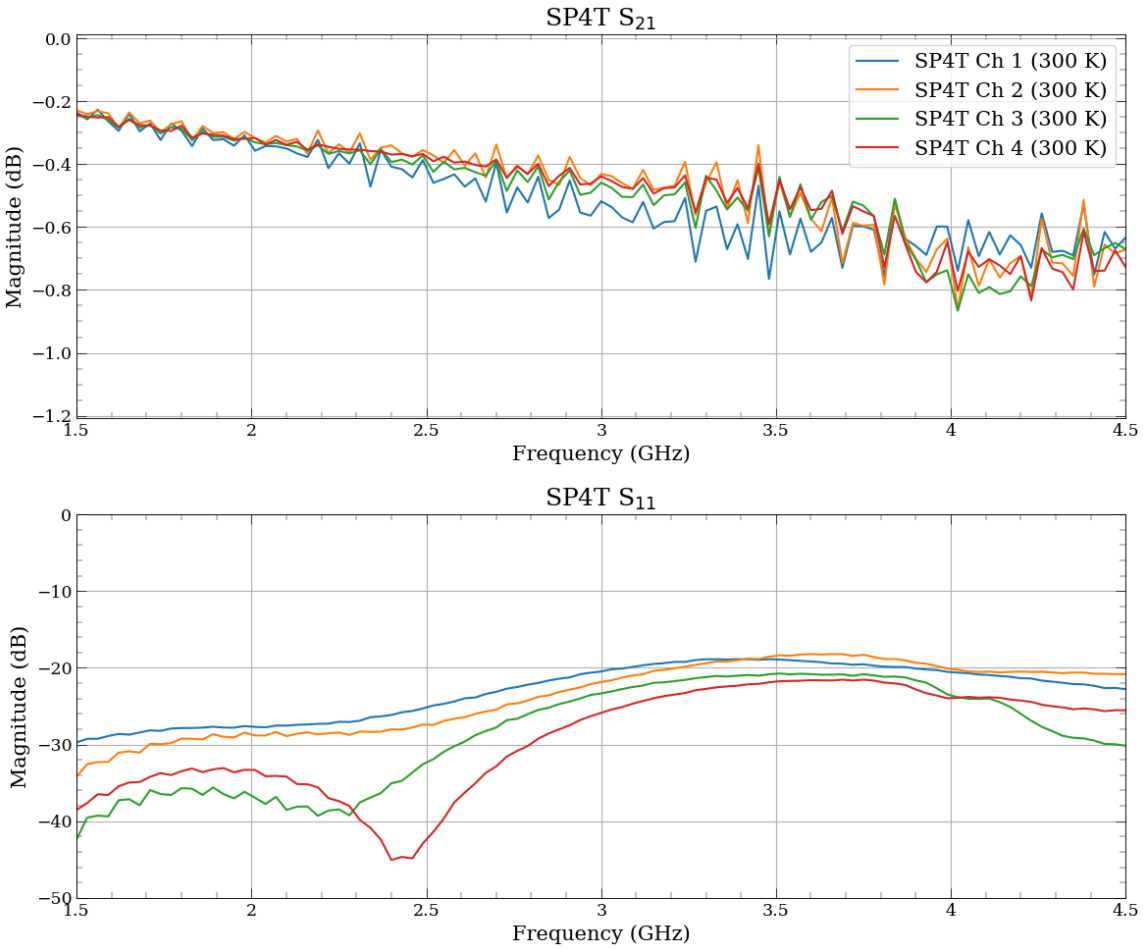

Figure 8. SP4T Individual Trace Performance

Note: Transmission and reflection data of the SP4T switch board calibrated by the ECAL. The S_{21} performance varies slightly and has to be shown on a much smaller scale than S_{11}. The reflections were not ideal or repeatable.

into the cryostat and wired through an external DC wire box. This was a Hammond box, shielded electrically and thermally. Thin cryo-wire connected to the switch via an adaptor. In that way the switchboard provided useful insight for the remote control aspects of the in-situ calibration but it was not used in the final cryogenic testing. I go over the future potential of the switch board in section 4.

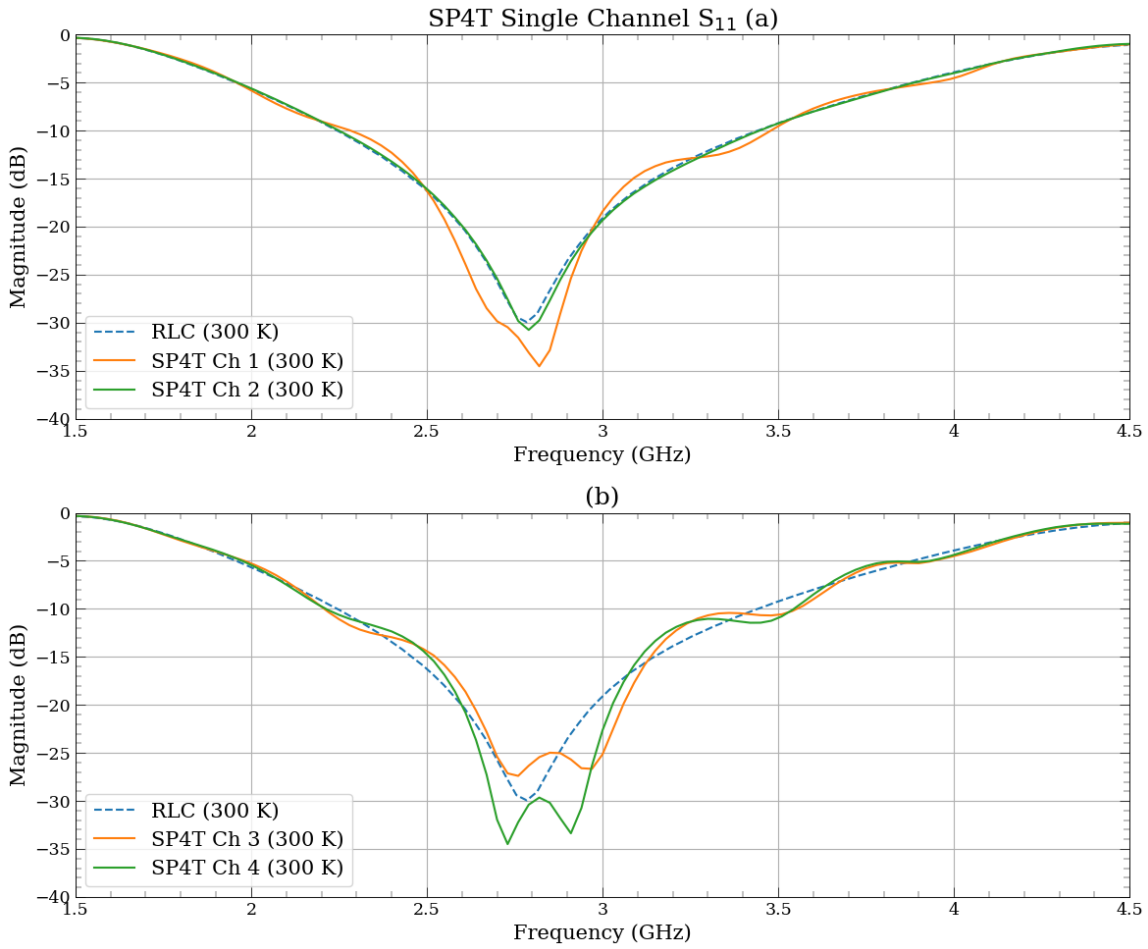

Figure 9. SP4T Single Channel Calibration

Note: Plot (a) shows the S_{11} data for the DUT in a dashed blue line compared to the de-embedded measurement through SP4T channel 2. The Ch 2 calibration was left and used to measure the DUT at Ch 1 as repeatability test. The only variation would be in the ports itself. Deviations are present. The same calibration of Ch 2 was shown to Ch 3, and 4 in plot (b). The S_{11} repeatability is not stable enough for a full in-situ calibration.

2.3 Flexible PCB

The flexible PCB approach was the method I was most eager to test. The boards originate from an earlier project where I designed novel flexible stripline based cryogenic transmission lines (Neric et al. 2020) for a NASA balloon mission. The PCB was an eight-channel transmission line in a single ribbon using planar technology to fit traces in parallel for a small form factor cable to replace bulky semi-rigid coax lines. A version can be seen in Figure 10. The flex lines were used in the IF chain of a heterodyne setup to transmit signal from an HEB mixer out of a cryostat. The layers of the PCB were prepared and bonded by Coast to Coast Circuits Inc. whose tolerances for physical trace dimensions were in the low 10 thousandths of an inch or better. The flex ribbons were designed so they could bond directly to vacuum flanges. This allowed all eight channels to be accessible outside of the cryostat. If trace repeatability was sufficient, then three channels of the flex circuit could be terminated with OSL standards and the remaining signal paths could be used for multiple DUTs. From outside of the cryostat an operator would manually move the VNA output from channel to channel which can partially be illustrated by Figure 11. The flex circuit was promising because the physical lengths of the individual traces inside the ribbon were very similar. The spacing between adjacent channels was already measured to have good isolation, some -50 dB over a 6 GHz BW. The connectors were SMP type so an SMA-SMP adapter was needed to attach to VNA cabling.

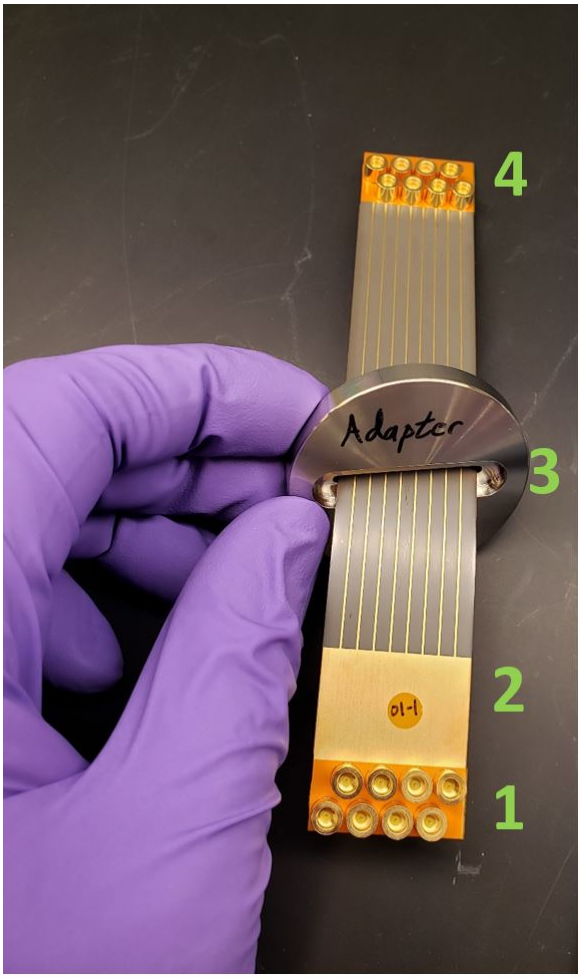

Figure 10. Flexible PCB Sample

Note: A short length of flexible PCB with eight stripline transmission line RF paths terminating in smooth bore SMP press on type connectors. The numbers correspond to the SMP connection sites (1, 4) an RFI shielding copper layer (2) and a vacuum flange (3). The flex circuit is bonded directly to the flange for vacuum use. The top ground strips are patterned from the same ground layer and are not signal carrying. The signal trace is buried under the substrate layer.

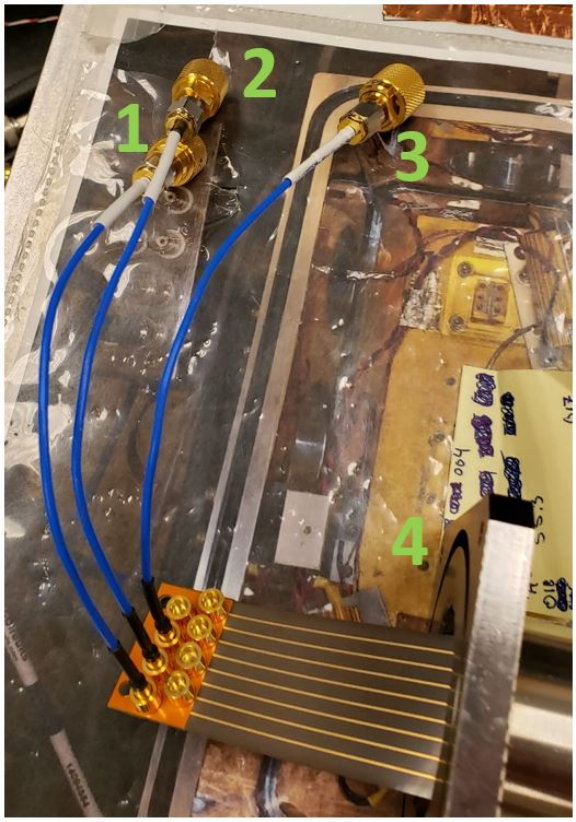

Figure 11. Flexible PCB Measurements

Note: A test setup of the flex circuit acting as a manual switch. The different internal channels can be accessed by physically moving the output port of the VNA to the corresponding external port. In this example reference standards for open-short-load (1-3) calibration are loaded on three of the circuits RF paths. The vacuum flange (4) would be normally installed into the wall of a cryogenic chamber. It is in open test configuration here. The visible portion of the circuit and call standards would be sealed inside a cryo chamber and thermally coupled to the testing stage. The channels of the flex circuit very in length for the top and bottom rows. There is approximately 240 mils of total physical length difference between the top and bottom rows.

The same VNA settings of the SP4T measurement were used to measure the flex lines. As before, a single channel calibration was carried out on a single channel (channel 1) of the flex circuit. The first result was good as was the case with the SP4T. The individual loss effects of a single channel could be de-embedded. There was one additional question to answer about the flex circuit. The press on connectors had to have a motion tolerance when they were snapped into place. This would prevent the center conductor of the SMP from breaking due to misalignment and repeated strain. There was concern that this added mechanical tolerance would have implications for the calibration error because the position of the cable would rest differently with each successive measurement. To test this I removed port 1 of the VNA from the input of channel 1 of the flex circuit after calibration was complete. I then simply re-applied it. For any type of connection this changes the environment of the cal by changing the position of the VNA cables. For SMA it would mean a difference in tightness of the connection site but the overall orientation of the coax would be unchanged. For SMP this meant a small angle deviation as well as pressure difference. Even with all that, a calibration should not vary more than a few dB. The major caveat here is that the flex circuit was designed for use in cryogenic measurements where their conductivity would improve so that S_{21} measurements rivaled coax at a 1/4 the thermal load. This meant that any room temp measurements would be extremely lossy due to the kapton substrate ($\epsilon_r = 4$). This could be mitigated somewhat by change the test power as high as 0 dBm at room temperature.

The second issue for this set of measurements was that the flex circuits used were "adapter" circuits made to test flight hardware. That means they were used heavily in the prototype process. The SMP connectors have a limited cycle of mate and de-mates before performance degrades. A nominal S_{21} difference between flex traces

is 10^{-2} dB, but here the deviation can reach as high as 10^{-1} dB for some of the more worn out paths. Another important factor to consider was that the even numbered channels of the flex had a different length than the odd. There was an approximate 240 mil difference in the layout so that the traces could be closely spaced but still accommodate the connector array.

Figure 12 shows the individual trace performance of channels 1, 3, 5, 7. Odd numbered channels meant equivalent lengths. The cables are extremely high loss at 300 K temperatures. These cables are also very short at 5 inches. Channel 1 shows the most wear from previous testing. DUT testing can be seen in Figure 13. The blue dashed line is the RLC measurement alone. The solid orange line was the DUT measurement after de-embedding channel 1. A second orange line with dashes and dots was the measurement of the same DUT with the same calibration, but I have disconnected and re-connected the DUT to flex Ch 1. This isolated the extent of the error from the press-on connector type because the DUT, and transmission line length were unchanged, only the orientation and pressure of the SMP joint was different. On that same plot I measured channel 3 with the same calibration. These two channels should have the same length. This measured the impact of three factors: (1) the press-on connector in addition to (2) variation in trace length from manufacturer tolerance and (3) device wear. Channel 3 was used an order of magnitude less often than channel 1 in prototyping. Figure 13(b) was made from data of channels 2, and 4. These were shorter than the odd numbered paths so this measurement was to more broadly emphasize the impact of trace length. Interestingly the deviation between even numbered channels that were calibrated by odd numbered ones is less of an impact than expected. Though 2, and 4 did not give the correct response, they were in better agreement with one another than in the SP4T case. It is important to note

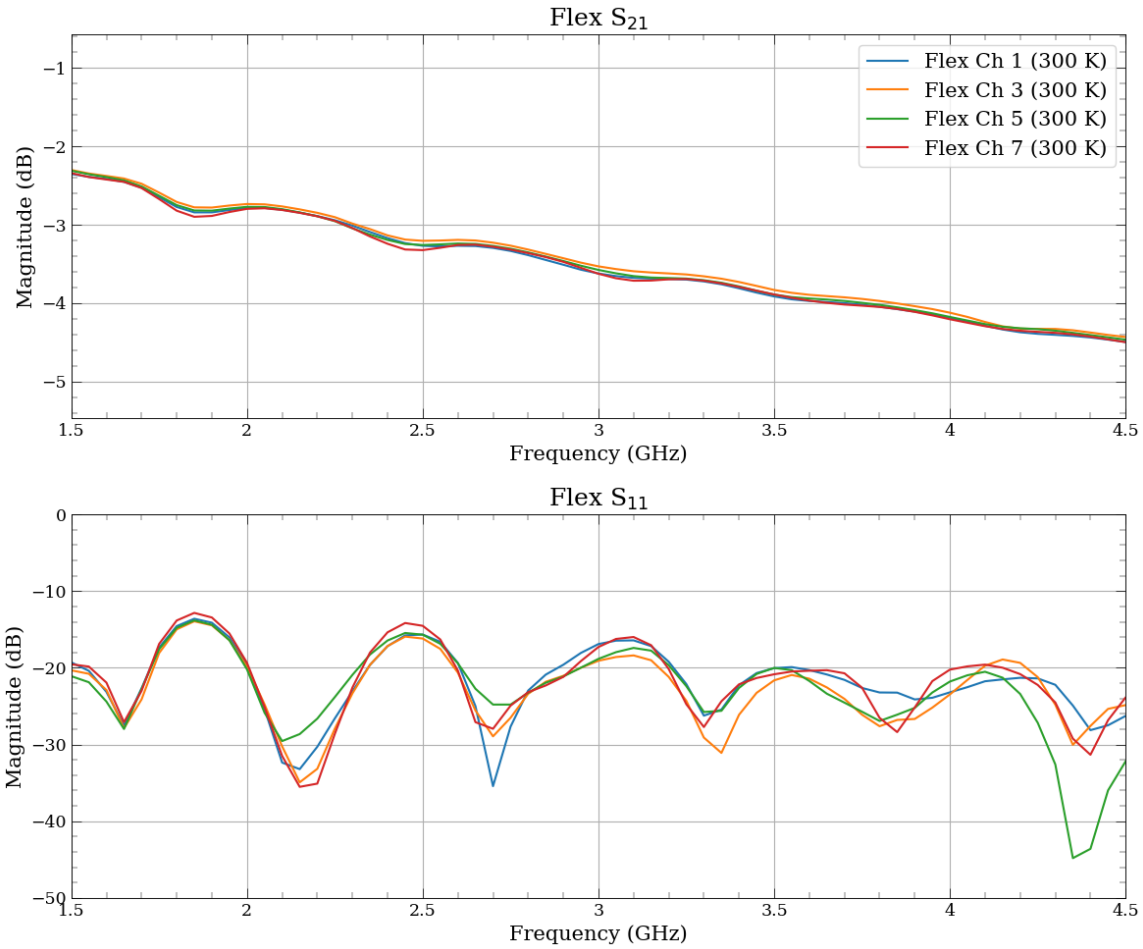

Figure 12. Flex Individual Trace Performance

Note: The S-parameters of a small length flexible adapter circuit. This one was heavily used in other projects for testing. The room temperature performance of a flex line suffers from a high loss substrate. The performance is greatly improved at lower temperatures where the conductivity of the transmission line is increased. The transmission seen in S_{21} is repeatable at these temperatures even though the loss is high, and the reflections have an appreciable impact. Though the circuit cannot serve its main purpose as an IF harness in this test configuration it was believed it might be an effect calibration network.

then, that trace repeatability is not the main issue with this setup. The connector wear is a larger contributor and with the press on nature driving up the error. I discuss possible solutions in 4.

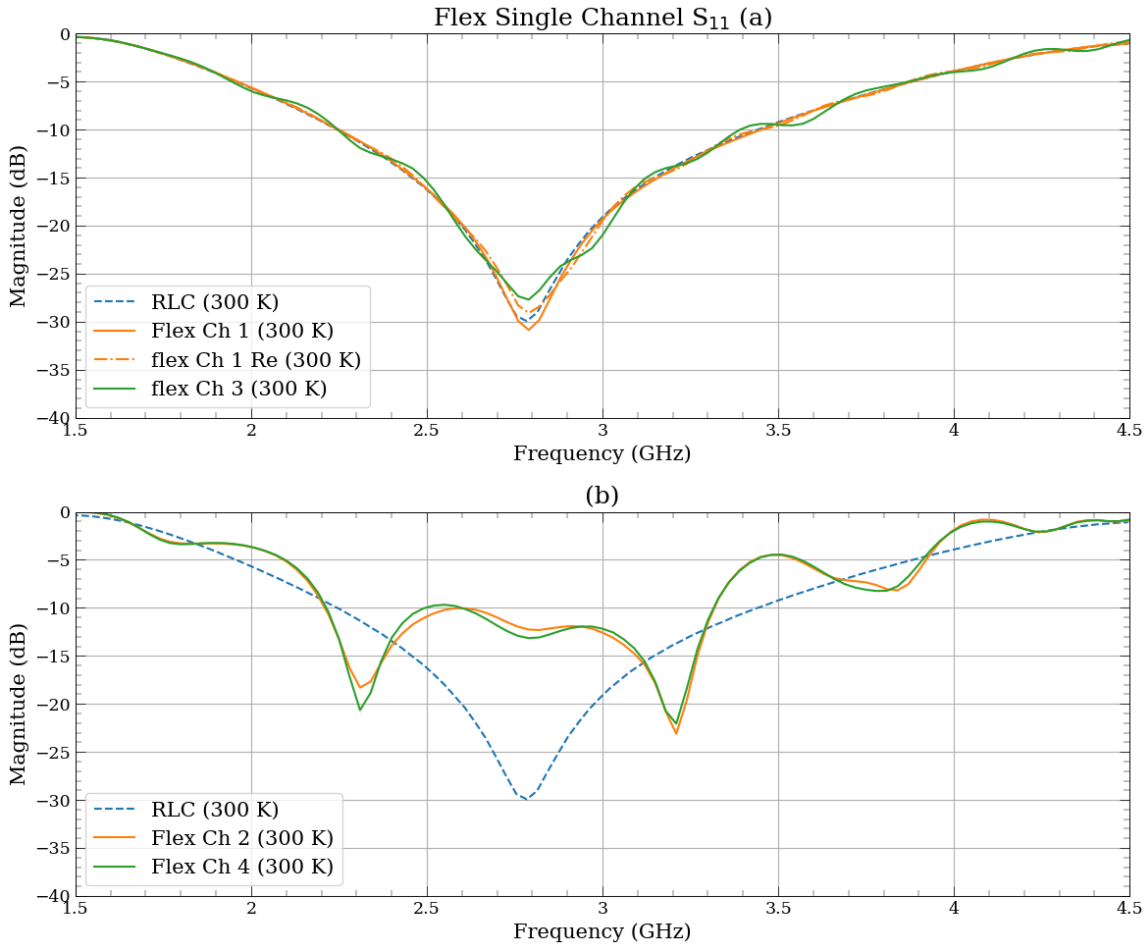

Figure 13. Flex Single Channel Calibration

Note: This data set is of the single channel calibration performance. The DUT was again a lab made RLC circuit. Ch 1 was the calibration point in solid orange. The added uncertainty from the press on connectors was investigated by making several mate and de-mates of channel 1 in (a). The orange dash-dot line shows the change in measurement from that action. Ch 3 is shown in plot (a) as well which is equivalent length to Ch 1. Fluctuations from a standing wave are caused by both the difference in connector orientation that is common in the SMP and the state of the connectors themselves. Plot (b) shows the Ch 2 (orange) and 4 (green) measurements using Ch 1 cal. These points are 240 mils shorter than channel 1 and not expected to look the same as plot (a).

2.4 COTS SP6T

The last approach was to use a commercial off the shelf Radiall R583423251 28V DC - 18 GHz SP6T barrel electrical mechanic latching switch. The difference between this and the previous barrel switch is that the R583 was designed for cryogenic use. The switch had a center SMA connector that was the common input and 6 encircling outputs. Seven DC bias lines powered the switch via a D-sub connector. This switch was an early model aquired from the manufacture for cryogenic testing. In order to bias the switch with available cryostats I had to wire a mating connector using cryo-wire. This was made slightly more complicated by the wire arrangement. In order to minimise the thermal load of the switch fewer DC lines were used to energise the RF path. That meant that each of the RF paths shared a bias wire with its neighbor. For example, to "turn on" Ch 1 a forward bias is applied bias 1 and bias 2. Reverse flow is used on the same bias points to "turn off" the path. Channel 2 shares bias 2 with channel 1 and bias 3 with channel 3. Turning on channel 2 requires forward flowing 28 V. If the bias was not floating, i.e. multiple pins shared the same ground then it was possible to energise two paths at the same time effectively making the measurement wrong. To access four RF paths required five pins which was possible with the 4 K test system. The switch with heat-sink can be seen in Figure 14.

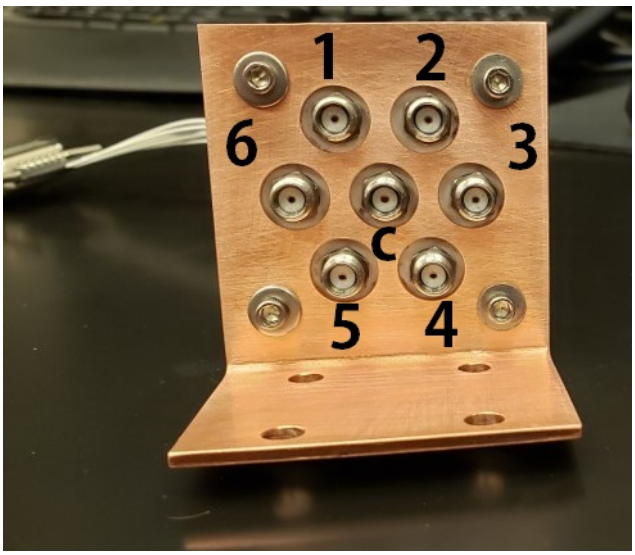

Figure 14. Radiall SP6T

Note: A Radiall R583423251 SP6T with copper heat bracket and DC bias lines. The common line in the center is labeled c where RF input can be switched to adjacent paths numbered 1-6.

The individual trace performance was outstanding. Figure 15 shows the transmission and reflection for channels 1, 2, 4, and 6. These were the ones used for in-situ testing because they were the easiest to attach to with the space provided. The single channel calibrating was carried out for switch channel 1 as the calibration point. That was compared to traces 2, 4, and 5 which was originally goin to be used in the cryo cal, but was replaced by channel 6. The results were in excellent agreement with the baseline RLC measurement. The data set was more uniform through the entire band and had overall less variance than either previous methods. The data can be seen in Figure 16. With that high confidence in hand a final room temperature test was done to characterise the DUT through the switch. The previous two methods yielded results that were non physical. For this measurement open, short, and load standards from the 85033D kit were loaded on to the SP6T channels 1, 2, and 3. The DUT was loaded on channel 4. The VNA was calibrated switching between standards using the same bias box network that would be used in the cryogenic cal. I measured the DUT itself when in-situ first. This was a rehearsal for the cryogenic measurements. This would also help identify any RF interconnects that were a potential issue in the cryostat network. I then installed the DUT along with the switch and standards in the vacuum chamber. I sealed it but did not pull a vacuum or reduce the temperature. Figure 17 is the resulting data plot. The dashed blue line is again the DUT measured by the VNA without any special preparation. The orange line is the measurement of the DUT through the VNA network. The solid blue line is the in-situ room temperature measurement of the RLC test circuit when sealed in the cryostat. The blue data set has an unexpected gain on the return loss near the resonance frequency but is otherwise stable throughout the rest of the BW. This blip was not an error, but may have been indicative of a cryostat TL bending or fraying between measurements. This

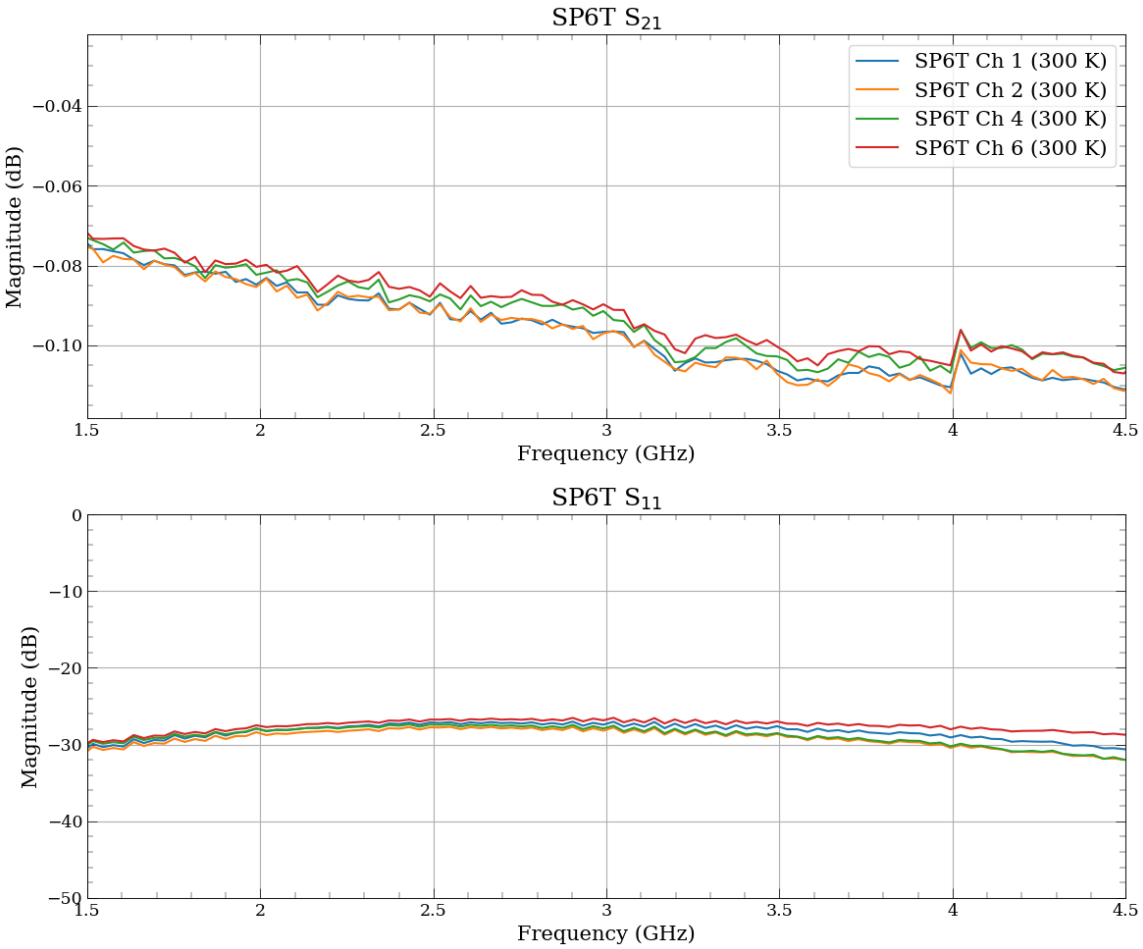

Figure 15. SP6T Individual Trace Performance

Note: The raw channel transmission and reflections of the Radiall SP6T. These traces showed the most consistency overall between the three room temperature tests. Ch 1, 2, 4, and 6 are shown here as they were the ones ultimately used in cryogenics calibration discussed in section 3.1.

feature is present in cryogenic data and validation set as well that will be discussed in the following section 3.1.

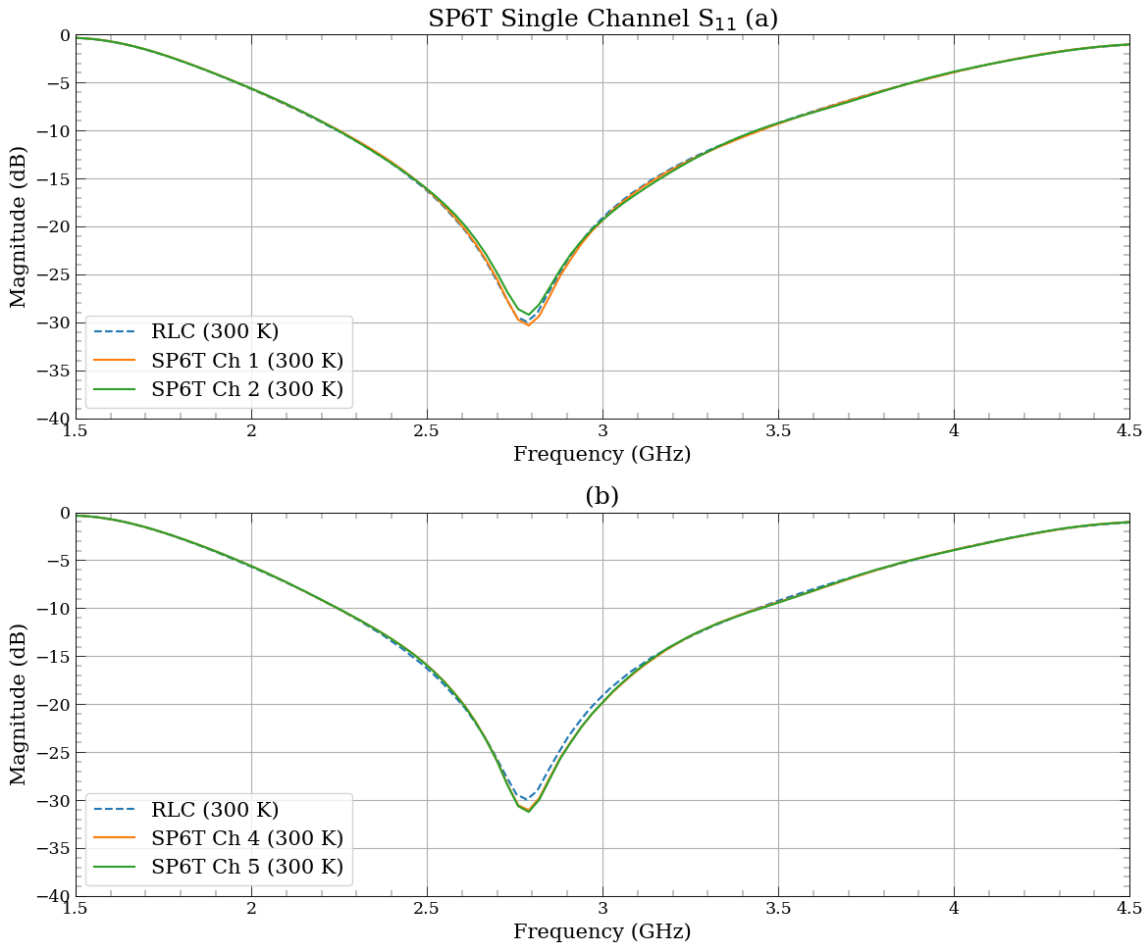

Figure 16. SP6T Single Channel Calibration

Note: SP6T Single channel calibration performance was immediately recognizable as the best performer. The same labeling scheme is used as with the pervious two setups. Here the trace repeatability is the closest to the actual measurement as seen from a qualitative look.

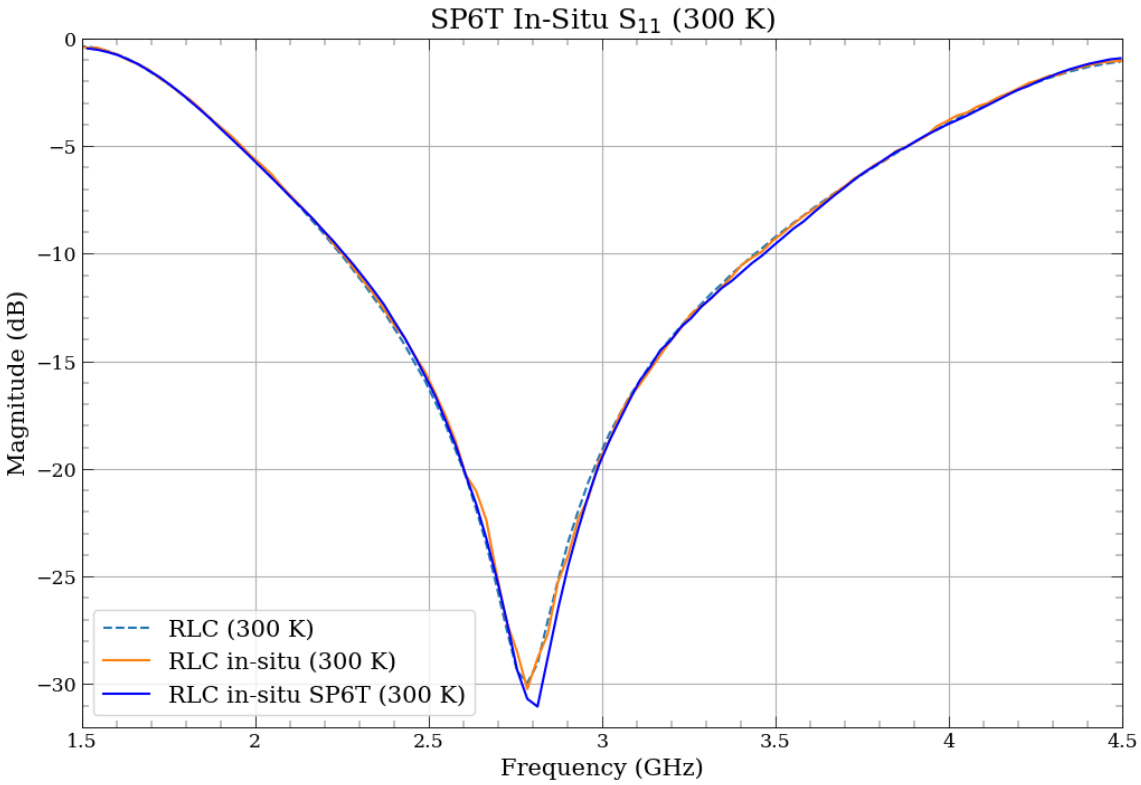

Figure 17. SP6T Room Temp In-Situ Calibration

Note: A series of in-situ tests were done prior to cryogenic testing. The RLC circuit was measured through the cryostat, seen as the solid orange trace, and compared to the DUT alone (dashed blue), and DUT in-situ measured through the switch which is the solid blue line.

Chapter 3

VACUUM CRYOGENIC RF CALIBRATION

3.1 Calibration Techniques

The SP6T was previously tested at a set of cryogenic temperatures by itself to document its optimal switch settings. I made an L shaped heat sink for the switch out of 80 mil thick oxygen free high conductivity copper and installed the switch in the chamber with the RF input through the cryostat using a hermetic feed through in the vacuum blank to connect to the switch common. The second port of the VNA was the switch output through a cryostat via another blank. The goal of this test was just to see the switching action so only one port was needed to check when the switch turned on or off. At room temperature the minimum pick up voltage was 18 V with a minimum actuating current of 39 mA. The max settings used were the manufacturer recommended 28 V with 61 mA current. As temperature decreased the voltage was slowly tuned down in 5 V increments and the switching mechanism was tested. It was expected that at lower temperature the device electronics would need lower voltage to reach actuating current. The goal of stepping down voltage was so that the current would not exceed 60 mA. At 11 K temperatures the minimum supplied voltage that resulted in the switch powering on was 0.88 V resulting in a current of 0.30 mA. This would not consistently activate an RF path probably due to temperature fluctuations. I found the optimal 11 K bias was 1.5 V with 48 mA which gave constant switching. A max voltage of 2 V was tested yielding 0.66 mA. Each pulse was short but it was still possible that the act of switching was temporarily increasing the internal temperature

of the SP6T. A Lakeshore temperature sensor was attached directly to the chassis of the switch which was thermally coupled with the external heat sink and therefore did not register any change in temperature due to switching. The switch was warmed up and tested again at room temperature and functioned within expected parameters.

The VNA settings for the in-situ cryogenic measurements were: test port power set to P = - 20 dBm. This was higher than initial room temperature testing to improve fidelity of results. The frequency span was from 0.10 - 6.00 GHz. The IF bandwidth was 10 HZ, and averaging was 16 times, up from 10, with 201 points. The SP6T was installed in the cryostat with a heat bracket. Short 6 inch mini circuits coaxial UT-45 hand formable cables were used as the interconnect between the switch and other components. The calibration standards, and DUT were originally intended to be installed on the same heat sink tower, but due to space constraints and concerns about damaging the mini circuits cables, they were split up. The UT-45 cables were thin and more fragile so they could not handle tough bend radii. The DUT and one standard were thermally coupled to the heat tower, while the remaining two standards were clamped directly to the test bed. An external DC power supply and a Hammond box with BNC inputs were used to supply power to the switch. Figure 18 shows the setup just before DC power is attached to the switch. The internal bias lines are twisted pair thin gauge cryowire. Port 1 of the VNA reached the inside of the crysotat with stainless-steel to stainless-steel coax cable. As was the case with the room temperature testing, I sealed the cryostat but did not pull a vacuum. I tested the bias, and measured the room temperature calibration first. The results were as expected so I moved on to cryogenic testing.

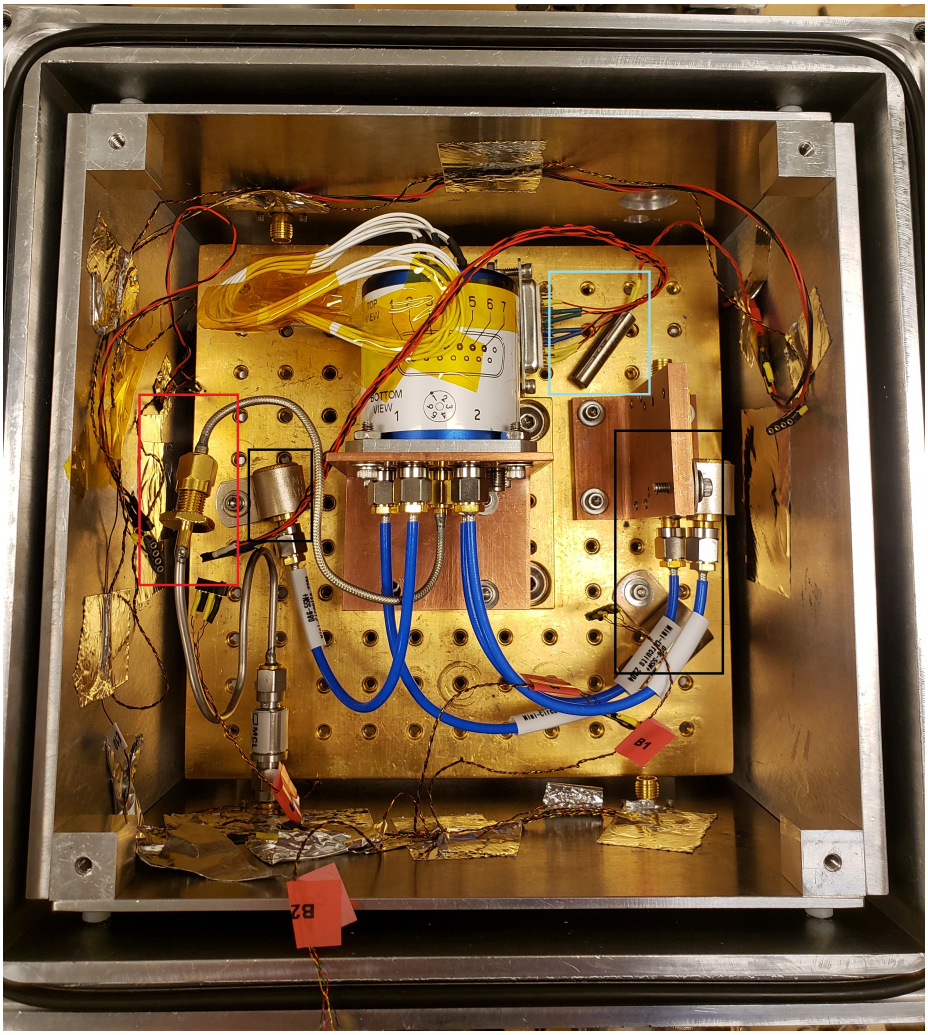

Figure 18. Cryogenic Calibration Test Set-up

Note: This image shows the test setup for the cryogenic in-situ calibration as the switch was being installed. The red box highlights the RF input from the VNA through SS coax cables that lead to the common of the SP6T. The black boxes show where the calibration standards have been thermally coupled to the 4 K cryogenic test bed. The teal box shows a resistive heater that was not used in testing but could be used to speed up the process.

For the cryogenic testing the vacuum cryostat was brought to $\sim$ 4 K temperatures and measurements began. I initially expected that 2 V would be sufficient to operate the switch, but at lower temperature there was a slight change in behavior. The nominal pickup voltage and current fluctuated between (2 - 4) V and (34 - 128) mA respectively. The 128 mA current was much higher than the expected 60 mA, but no obvious sings of damage to the switch were observed. The pulse time was $\sim$ 1 second. The room temperature calibration that was done before cryogenic testing was left unchanged. It would no longer yield a realistic physical response for the DUT at cryogenic temperatures. When the test bed stabilized at 3.3 K I repeated the VNA calibration in-situ. The Lakeshore sensor was monitored closely as the reference standards were measured, just in case the switching bias raised the temperature. If there was any change in temp, the averaging of the VNA would be paused and restarted until the temp fell back to 3.3 K. The benefit of the in-situ method was that at any point the calibration could be repeated. The RLC response was recorded and compared to the room temperature calibration. After a few minutes of delay, the measurement was taken again to roughly the same effect. Change in the IF bandwidth also had no obvious impact on the results. That data will be shown in section 3.2.

At the conclusion of the in-situ test I needed some measurement to validate that the cryogenic one was a success. Recalling the manual technique used in Rodriguez-Morales, Yngvesson, and Gu (2010), I repeated the setup. I removed the SP6T and accompanying heat brackets. I installed only the open circuit directly at the center of the system. I then brought the system to cryogenic temperatures, but this time there was sufficiently less material inside the cryostat and the temperature would go below 3 K. Large resistors in the cryostat could be used as heaters to either quickly warm up a cryostat after a cool-down, or (using low power) to stabilize the test bed at a higher

than normal temperature. Since this heater was not used in the SP6T testing, I chose to leave it off and instead start the VNA averaging when the cryostat approached 3.3 K. This resulted in a small fluctuation in temperature due to the time it took for the VNA to average the response 16 times. I chose not to reduce the averaging though, to make sure the two cryo test were as close as possible with regards to setup. There were already some anticipated factors that would that add uncertainty to the manual method such as RF cable positioning, and temperature sensor placement varying when replacing standards. The difference in thermal load and averaging time were additional factors that highlight the mechanical improvements of the SP6T in-situ setup. The manual method took 3 cycles to calibrate spanning roughly 2 days, and 1 cycle to measure the DUT. Table 1 shows the testing schedule. This particular cryostat is considered fast. Many larger setups would take days for a single cycle rather than a scale of several hours. Figure 19 shows the setup for one of the individual calibration standards. Data is discussed in section 3.2.

Table 1. Manual Method Test Schedule

Obj	Date	Time	Temp Range (K)
Open	5/6/2022	1516	3.37 - 3.28
Short	5/7/2022	1230	3.33 - 3.26
Match	5/7/2022	1800	3.32 - 3.20
DUT	5/8/2022	1335	3.33 - 3.27
DUT	5/8/2022	1405	2.99 - 2.97

Note: This table is the schedule of events that culminated in the manual in-situ calibration. It took 4-cycles over several days to achieve the measurement. The First three objects measured were for calibration. The fourth object was the RLC DUT at the approximate 3.3 K temperature that the single cycle SP6T cal measured. The last entry was measuring the DUT again to show how much the calibration drifted as temperature continued to decrease. The range of temperatures comes from the different thermal load on the test bed, and the averaging time of the VNA.

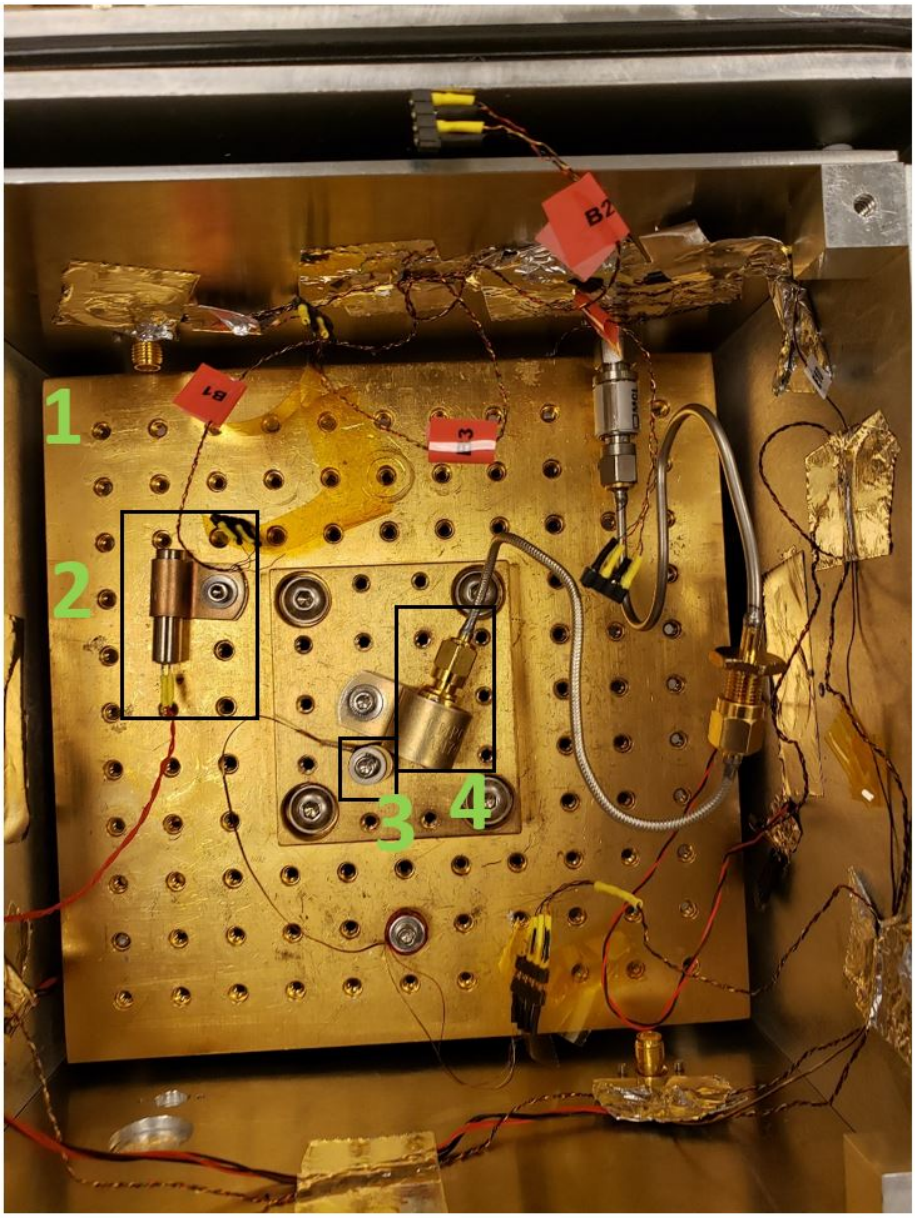

Figure 19. Manual Cryo Cal

Note: A multi cycle manual calibration was used in order to validate the SP6T in-situ cal. Pictured here is the 4 K cryogenic test bed. The 4 K cold plate is labeled with a 1. The cryostat heater is labeled 2 and outlined with a black box. The temperature sensor is in box 3. and the individual calibration standard for that run is in box 4.

3.2 Results

The first important results are the direct comparison of the SP6T in-situ cryogenic measurement to the SP6T in-situ at room temperature of that DUT. In Figure 20 that data is plotted on a rectangular plot. The solid blue is the DUT as measured inside the crysotat through the SP6T prior to the cryo cycle. The pink dashed line is the SP6T method at 3.3 K. Right away there is an obvious change in response where the resonant frequency has shifted to a higher value from 2.80 GHz to $\sim$ 2.85 GHz. The shift was anticipated. The resonant frequency $f_0 = \left(\sqrt{\text{LC}}\right)^{-1}$ is directly effected by the value of inductance L and capacitance C. These values come from the intrinsic properties of the circuit elements and transmission lines, and are each proportional to the ratio of area to length of the components. There will be a physical contraction at lower temperatures tending to drive the overall values of C and L. The fact that they are both proportional to [m^2] / [m] will mean that the change is slight but ultimately L and C will decrease and f_0 will conversely increase. The materials used in the circuit matter for this change as well and will vary from manufacturer. From 300 K to 3.3 K a nearly 100 $\times$ difference in temperature saw a $\sim$ 3.5% decrease in the ratio LC. The general curve of the response is also smooth and without ripple. This was not the case when a thermal calibration was used to measure the RLC at cryo. There a standing wave would plague the measurement. The validation step was to add to this plot the measurement from the manual method. The dashed brown trace shows the RLC circuit measurement after a manual 4 cycle calibration. The two cryo measurements are in good agreement. The mean average of both measurements yielded a standard deviation $\sigma = 0.25$ dB as the upper and lower bounds of the data.

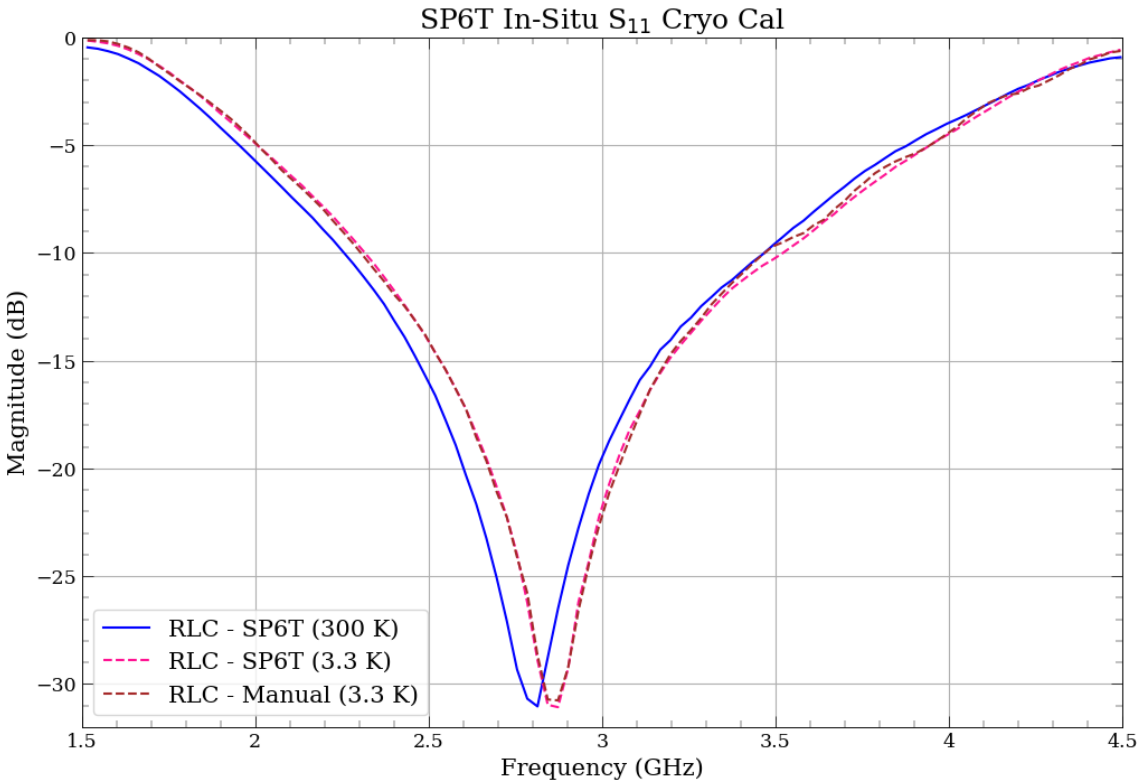

Figure 20. Cryogenic Vacuum In-situ Measurement: RLC

Note: A basic RLC circuit measured at room temperature 300 K (blue), and at 3.3 K using RF switches (pink) and manually calibrating standards (brown).

There are some visually obvious differences at the natural frequency and at higher frequencies.

Of course these measurements were meant to lead to a complex impedance so the plot is redone as a smith chart in Figure 21. As mentioned in section 3.1 the removal of the switch in the manual method caused the final temperature of the chamber to drop below 3.3 K. Since this was the SP6T reference temperature it was imperative that the manual method be done at the same point. The calibration standards were measured over a temperature range near that value. A big motivator in this work was doing lower temperature calibrations so that one would not have to rely on a factory or room temperature cal that is unstable when the thermal conditions change. Up until now that difference was usually from calibrating the VNA at 300 K and measuring at $\sim$ 10 K. It is still the case, that a calibration at 3 K would not hold for a measurement at 2 K or vice-versa. This point is illustrated in Figure 22. The measurement of the DUT that was taken at 3.3 K can be seen in the brown dashed trace. The cryogenic system was left on for some time longer. The cold plate reached 2.9 K and another measurement was recorded, which is the light brown trace. Here it is visually obvious that there is an erroneous calibration drift. What is most problematic is that without a heating mechanism, the measurement window for the desired temperature can close and be missed. This would result in either a full abort or the test will have to be repeated by turning off the cryo compressor, allowing a higher temp to be reached and turning the compressor back on again. It is recommended that repeated short time start/stop cycles of the compressor are avoided to increase the life of the equipment. This was not a problem for the SP6T where I was able to do repeated calibrations at will. Should the temperature change for any reason with this setup it would be only the slightest inconvenience.

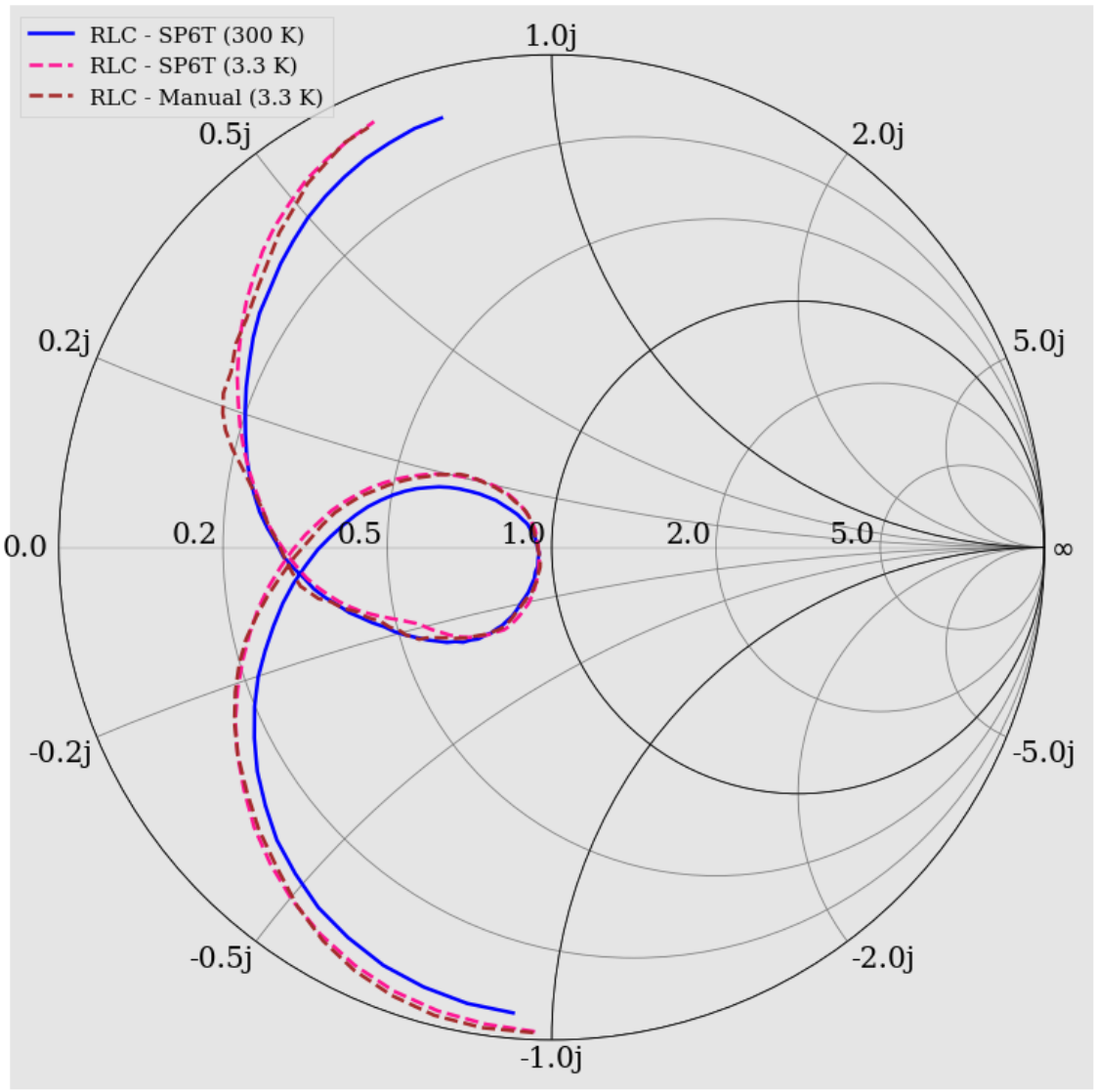

Figure 21. RLC Impedance Smith Chart

Note: A smith chart representation of the S_{11} measurements from figure 20. As before the room temperature 300 K is represented by a blue trace. This time I used dashed lines to represent the 3.3 K RF switch calibration in pink and manually calibrating standards are dashed brown for ease of visualization.

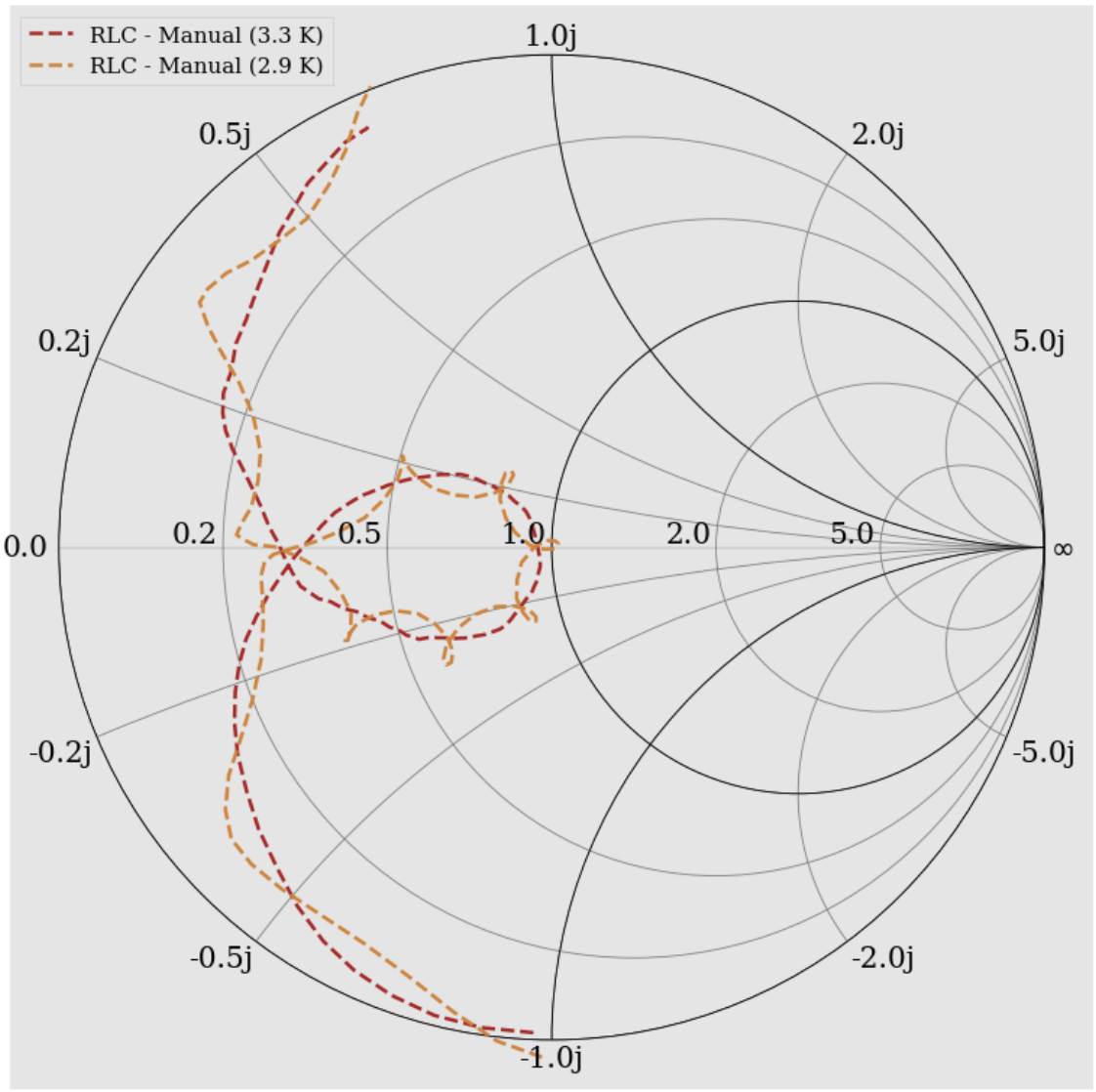

Figure 22. Impedance Drift

Note: This smith chart shows the manual calibration again from figure 21 as the same dashed brown line. Plotted against it is the calibration drift. This occurs when the 3.3 K calibration is not updated and temperature changes. The second light brown plot is a measurement of the RLC at 2.9 K with a 3.3 K calibration.

Chapter 4

FUTURE WORK

The success of the SP6T method is only the first step in making a general purpose in-situ setup. It was an effective approach that reduced OSL cycles from four down to one, and added the benefit of re-calibration in that same cycle. The drawbacks were that the setup required a lot of space which is often limited in cryostats. The switch itself was bulky and added to the thermal load of the test stage. The switch may also not be ideal for measurements involving magnetic fields. Despite this, the SP6T can be used to make accurate characterizations of connectorized devices, and it may also serve as a baseline for identifying the viability of new techniques. From the SP6T individual trace performance one can see the importance of S_{11} repeatability is critical to measurement accuracy. The other two methods investigated in this work did not achieve a desired result but they are not out of the game yet.

The next steps for the SP4T switch board are to investigate the individual SPDT S-parameter performance on an evaluation board. One such board was provided by the manufacturer and used to test an individuals switch performance, but by using it to test all three, one can separate any parasitic behavior of the circuit board and connectors. Should the switch repeatability prove as good or better than the SP6T, then the issues observed with that setup will have been from the PCB itself. Modifying the switchboard RF paths so that they terminate on the far side of the board away from the common can definitively alleviate any interference or cross talk from the input alone. The paths would be gradually curved, or make use of miter lines to guarantee an impedance match across the network. An enclosure housing should be

built to further shield the CPW paths from outside interference. Side mount SMA connectors should be used, which would fasten to the enclosure first rather than grip the sides of the board unevenly. They would have only one solder contact with the PCB which reduces the overall metal content of the board that might lead to further impedance mismatch.

The flex circuit also has a three clear paths forward. One straightforward approach would be to replace the SMP press on type of connectors with a surface mount SMA, or another connector type that can be fastened rather than relying on a single point of non uniform contact. This might require some rework of the flex line terminations and lead to further simulations, but ultimately could be worth it because the ribbons do not take up as much space as the switch and ultimately add more channels to the vacuum chamber. This method does not require extra biasing and will not likely interfere with magnetic measurements. A second solution which is perhaps the easiest to test going forward would be to use the SP6T or even another pre-built barrel type SP4T switch at room temperature external to the system and connect through the cryostat via flex lines. The flex ribbons are slow at transferring heat, so the cryogenic system would be able to keep up. The DC for the switch would be external as well and require less effort to actuate. A third path which is a combination approach of flex and switch can also be factored in to the flex circuit design. It is, after all, a PCB by nature and built in layers. Lands for a set of SPDTs could be placed at the flex circuit terminus. CPW or microstrip lines could bring the RF paths out of the switches and to a side mount input port. This is of course if the SPDTs used are repeatable as mentioned above. An external switching mechanism could also lead to an electronic cryogenic calibration setup since it would be control electronics that fail at cryogenic tmps. The flex circuit was designed to attach to LNA breakout board

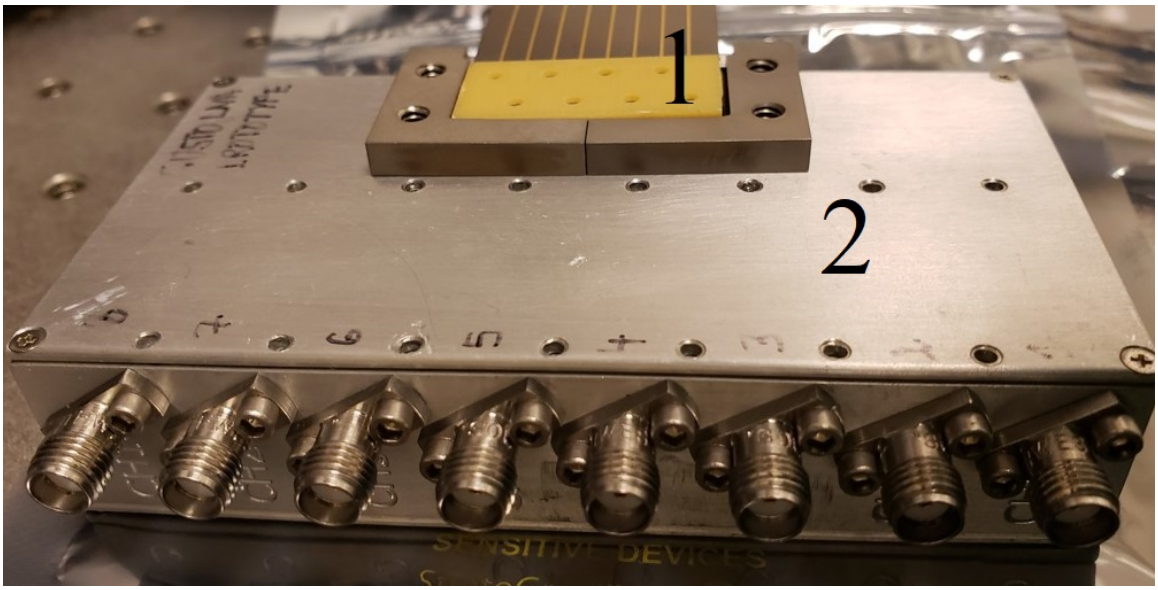

Figure 23. Flex Circuit Breakout

Note: An example of a flex circuit (1) connected to a DC breakout board powering 8 LNAs in an enclosure housing (2). The LNAs RF output exits through side panel SMA connectors. It may be possible to use a similar setup to avoid error from the SMP press on connectors.

housed in an enclosure box. This example of the flex versatility may also solve the connector problem. An image of the flex circuit attached to the LNA box can be seen in Figure 23. Here the terminations are SMA and more reliable than the SMP type for calibration. The flex circuit need not be modified in this case, by simply adding a breakout board with or without DC power, that rests external to the cryostat which would allow for manual switching. The internal part of the flex could remain unchanged as it is not moving while inside the chamber.

The impetus for this work was to measure the temperature and frequency dependent complex impedance of an HEB. That process is still on going. In this work I have shown that a standard RLC circuit can be measured at cryogenic temperatures in-situ with an SP6T. This was the general purpose case. In my dissertation I will show how the SP6T method was used to measure a superconducting element of a non-linear detector. That was ultimately the last step before the actual HEB testing. The HEB has not been measured yet due to several factors. The first is that the cryostat test setup must be expanded to include a "window". In the case of cryogenics that is a thin sheet of Mylar transparent plastic. The window will allow optical pumping of the HEB. That is to say a THz LO will act as the sky source and lab source to drive the HEB and output a simulated response. The next important element would be to design and deploy a bias-tee that provides DC bias input and RF output for the HEB. Of course the measurement depends on a working HEB which is not available for testing at this time.

The conclusion for now is that the SP6T is the best working solution going forward for measuring devices like NbN HEB mixers under operating conditions. This method could provide the most accurate measure of impedance to date. The accurate impedance measure is the missing piece to developing a stable matching networks for the HEB, and increasing accuracy and sensitivity of THz astronomical measurements.

REFERENCES

Couëdo, F., L. Bergé, L. Dumoulin, M. Aprili, C. A. Marrache-Kikuchi, and J. Gabelli. 2019. "Sample-based calibration for cryogenic broadband microwave reflectometry measurements." *AIP Advances* 9 (7). https://doi.org/10.1063/1.5097897.

Cunnane, Daniel, Jonathan Kawamura, Boris S. Karasik, Matthaeus A. Wolak, and X. X. Xi. 2014. "Development of hot-electron THz bolometric mixers using MgB 2 thin films," vol. 9153. https://doi.org/10.1117/12.2054607.

Diego, Juan Cano de. 2010. "Cryogenic Technology in the Microwave Engineering: Application to MIC and MMIC Very Low Noise Amplifier Design." *Tesis Doctorales en Red (TDR).*

Ekström, Hans, Boris S. Karasik, Erik L. Kollberg, and K. Sigfrid Yngvesson. 1995. "Conversion Gain and Noise of Niobium Superconducting Hot-Electron-Mixers." *IEEE Transactions on Microwave Theory and Techniques* 43 (4). https://doi.org/10.1109/22.375258.

Fromm, W. E. 1955. "Characteristics and some applications of stripline components." *IRE Transactions on Microwave Theory and Techniques* MTT-3 (2). https://doi.org/10.1109/TMTT.1955.1124912.

Gousev, Yu P., G. N. Gol'Tsman, A. D. Semenov, E. M. Gershenzon, R. S. Nebosis, M. A. Heusinger, and K. F. Renk. 1994. "Broadband ultrafast superconducting NbN detector for electromagnetic radiation." *Journal of Applied Physics* 75 (7). https://doi.org/10.1063/1.356060.

Khosropanah, P., J. R. Gao, W. M. Laauwen, M. Hajenius, and T. M. Klapwijk. 2007. "Low noise NbN hot electron bolometer mixer at 4.3 THz." *Applied Physics Letters* 91 (22). https://doi.org/10.1063/1.2819534.

Kooi, J. W., J. J.A. Baselmans, M. Hajenius, J. R. Gao, T. M. Klapwijk, P. Dieleman, A. Baryshev, and G. De Lange. 2007. "IF impedance and mixer gain of NbN hot electron bolometers." *Journal of Applied Physics* 101 (4). https://doi.org/10.1063/1.2400086.

Kurokawa, K. 1965. "Power Waves and the Scattering Matrix." *IEEE Transactions on Microwave Theory and Techniques* 13 (2). https://doi.org/10.1109/TMTT.1965.1125964.

Mani, Hamdi, and Philip Mauskopf. 2014. "A single-stage cryogenic LNA with low power consumption using a commercial SiGe HBT." https://doi.org/10.1109/WOLTE.2014.6881015.

Merkel, Harald. 1999. "A hot-spot mixer model for phonon-cooled nbn hot electron bolometric mixers." *IEEE Transactions on Applied Superconductivity* 9 (2 PART 3). https://doi.org/10.1109/77.783951.

Nebosis, R. S., Yu. P. Semenov, and K. F. Renk. 1996. "Rigorous Analysis of a Superconducting Hot-Electron Bolometer Mixer: Theory and Comparison with Experiment."

Neric, Marko, Christopher E. Groppi, Hamdi Mani, Justin Mathewson, Kristina Davis, Matthew Underhill, Craig Kulesa, Christopher Walker, Thomas Mozdzen, and Abram Young. 2018. "IF system design for the Galactic/Extragalactic ULDB Spectroscopic Terahertz Observatory (GUSTO)," 101. https://doi.org/10.1117/12.2314096.

Neric, Marko, Hamdi Mani, Thomas Mozdzen, and Chris Groppi. 2019. "Design and Prototyping of New Flexible Stripline based Transmission Lines as Alternatives to Semi-Rigid Coaxial Cables." In *ISSTT 2019 - 30th International Symposium on Space Terahertz Technology, Proceedings Book,* 69–71.

Neric, Marko, Hamdi Mani, Thomas Mozdzen, and Chris Groppi. 2020. "Characterization of cryogenic flexible transmission lines designed for the GUSTO if harness." In *Proceedings of the 31st Symposium on Space Terahertz Technology, ISSTT 2020,* 50–53.

Pozar, David M. 2011. *Microwave engineering.*

Ranzani, Leonardo, Lafe Spietz, Zoya Popovic, and José Aumentado. 2013. "Two-port microwave calibration at millikelvin temperatures." *Review of Scientific Instruments* 84 (3). https://doi.org/10.1063/1.4794910.

Ranzani, Leonardo, Lafe Spietz, Zoya Popovic, and Jose Aumentado. 2012. "A 4:1 transmission-line impedance transformer for broadband superconducting circuits." *IEEE Transactions on Applied Superconductivity* 22 (5). https://doi.org/10.1109/TASC.2012.2202116.

Rodriguez-Morales, Fernando. 2007. "Modeling and Measured Performance of Integrated Terahertz HEB Receivers and Focal Plane Arrays."

Rodriguez-Morales, Fernando, and K. Sigfrid Yngvesson. 2003. "Impedance and Bandwidth Characterization of NbN Hot Electron Bolometric Mixers."

Rodriguez-Morales, Fernando, K. Sigfrid Yngvesson, and Dazhen Gu. 2010. "Wide-band if-integrated terahertz HEB Mixers: Modeling and characterization." *IEEE Transactions on Microwave Theory and Techniques* 58 (5 PART 1). https://doi.org/10.1109/TMTT.2010.2045566.

Rytting, Douglas Kent. 2001. "Network Analyzer Accuracy Overview." https://doi.org/10.1109/ARFTG.2001.327486.

Slichter, Daniel Huber. 2011. "Quantum Jumps and Measurement Backaction in a Superconducting Qubit." *Doctoral Thesis.*

Spietz, Lafe, Kent Irwin, Minhyea Lee, and Jośe Aumentado. 2010. "Noise performance of lumped element direct current superconducting quantum interference device amplifiers in the 4-8 GHz range." *Applied Physics Letters* 97 (14). https://doi.org/10.1063/1.3497008.

Weinreb, Sander, Joseph C. Bardin, and Hamdi Mani. 2007. "Design of cryogenic SiGe low-noise amplifiers." *IEEE Transactions on Microwave Theory and Techniques* 55 (11). https://doi.org/10.1109/TMTT.2007.907729.

Yeh, Jen Hao, and Steven M. Anlage. 2013. "In situ broadband cryogenic calibration for two-port superconducting microwave resonators." *Review of Scientific Instruments* 84 (3). https://doi.org/10.1063/1.4797461.

Zmuidzinas, Jonas, and Paul L. Richards. 2004. "Superconducting detectors and mixers for millimeter and submillimeter astrophysics," vol. 92. https://doi.org/10.1109/JPROC.2004.833670.